Title
Physical Model Tests of Half-Scale Geosynthetic Reinforced Soil Bridge Abutments. II: Dynamic Loading

Journal
Journal of Geotechnical and Geoenvironmental Engineering, 145(11)

ISSN
1090-0241

Authors
Zheng, Yewei
McCartney, John S
Shing, P Benson
et al.

Publication Date
2019-11-01

DOI
10.1061/(asce)gt.1943-5606.0002158

Peer reviewed

Journal of Geotechnical and Geoenvironmental Engineering

Physical Model Tests of Half-Scale Geosynthetic Reinforced Soil Bridge Abutments. II: Dynamic Loading

--Manuscript Draft--

Manuscript Number:	GTENG-7259R2
Full Title:	Physical Model Tests of Half-Scale Geosynthetic Reinforced Soil Bridge Abutments. II: Dynamic Loading
Manuscript Region of Origin:	UNITED STATES
Article Type:	Technical Paper
Funding Information:	California Department of Transportation — John McCartney Federal Highway Administration — John McCartney
Abstract:	This paper presents experimental results from shaking table tests on four half-scale geosynthetic reinforced soil (GRS) bridge abutment specimens constructed using well-graded angular backfill sand, modular facing blocks, and uniaxial geogrid reinforcement to investigate the effects of applied surcharge stress, reinforcement vertical spacing, and reinforcement tensile stiffness for dynamic loading conditions. Similitude relationships for shaking table tests in a 1g gravitational field were used to scale the specimen geometry, applied surcharge stress, soil modulus, reinforcement tensile stiffness, and characteristics of the earthquake motions. Reinforcement vertical spacing and reinforcement tensile stiffness had the most significant effects on the maximum dynamic and residual wall facing displacements and bridge seat settlements. Acceleration amplification increased with elevation in the reinforced and retained soil zones. Residual vertical and lateral soil stresses were lower than the calculated values for static loading conditions. The maximum tensile strain in each reinforcement layer occurred near the facing block connection for lower layers and under the bridge seat for higher layers. The vertical seismic joint between the bridge beam and bridge seat closed during the Northridge motion, resulting in contact force. A companion paper presents experimental results for the same GRS bridge abutment specimens under static loading conditions.
Corresponding Author:	Yewei Zheng, PhD Old Dominion University Norfolk, Virginia UNITED STATES
Corresponding Author E-Mail:	y1zheng@odu.edu;zhengyewei@gmail.com
Order of Authors:	Yewei Zheng, PhD John McCartney Benson Shing Patrick Fox
Additional Information:	
Question	**Response**
Authors are required to attain permission to re-use content, figures, tables, charts, maps, and photographs for which the authors do not hold copyright. Figures created by the authors but previously published under copyright elsewhere may require permission. For more information see http://ascelibrary.org/doi/abs/10.1061/9780784479018.ch03. All permissions must	No

be uploaded as a permission file in PDF format. Are there any required permissions that have not yet been secured? If yes, please explain in the comment box.	
ASCE does not review manuscripts that are being considered elsewhere to include other ASCE Journals and all conference proceedings. Is the article or parts of it being considered for any other publication? If your answer is yes, please explain in the comments box below.	No
Is this article or parts of it already published in print or online in any language? ASCE does not review content already published (see next questions for conference papers and posted theses/dissertations). If your answer is yes, please explain in the comments box below.	No
Has this paper or parts of it been published as a conference proceeding? A conference proceeding may be reviewed for publication only if it has been significantly revised and contains 50% new content. Any content overlap should be reworded and/or properly referenced. If your answer is yes, please explain in the comments box below and be prepared to provide the conference paper.	No
ASCE allows submissions of papers that are based on theses and dissertations so long as the paper has been modified to fit the journal page limits, format, and tailored for the audience. ASCE will consider such papers even if the thesis or dissertation has been posted online provided that the degree-granting institution requires that the thesis or dissertation be posted. Is this paper a derivative of a thesis or dissertation posted or about to be posted on the Internet? If yes, please provide the URL or DOI permalink in the comment box below.	Yes
If yes, please provide the URL or DOI permalink in the comment box below. as follow-up to "ASCE allows	https://escholarship.org/uc/item/0vg5b2g4

submissions of papers that are based on theses and dissertations so long as the paper has been modified to fit the journal page limits, format, and tailored for the audience. ASCE will consider such papers even if the thesis or dissertation has been posted online provided that the degree-granting institution requires that the thesis or dissertation be posted. Is this paper a derivative of a thesis or dissertation posted or about to be posted on the Internet? If yes, please provide the URL or DOI permalink in the comment box below."	
Each submission to ASCE must stand on its own and represent significant new information, which may include disproving the work of others. While it is acceptable to build upon one's own work or replicate other's work, it is not appropriate to fragment the research to maximize the number of manuscripts or to submit papers that represent very small incremental changes. ASCE may use tools such as CrossCheck, Duplicate Submission Checks, and Google Scholar to verify that submissions are novel. Does the manuscript constitute incremental work (i.e. restating raw data, models, or conclusions from a previously published study)?	No
Authors are expected to present their papers within the page limitations described in <u><i>Publishing in ASCE Journals: A Guide for Authors</u></i>. Technical papers and Case Studies must not exceed 30 double-spaced manuscript pages, including all figures and tables. Technical notes must not exceed 7 double-spaced manuscript pages. Papers that exceed the limits must be justified. Grossly over-length papers may be returned without review. Does this paper exceed the ASCE length limitations? If yes, please provide justification in the comments box below.	No
All authors listed on the manuscript must have contributed to the study and must approve the current version of the manuscript. Are there any authors on the paper that do not meet these criteria? If	No

the answer is yes, please explain in the comments.	
Was this paper previously declined or withdrawn from this or another ASCE journal? If so, please provide the previous manuscript number and explain what you have changed in this current version in the comments box below. You may upload a separate response to reviewers if your comments are extensive.	No
Companion manuscripts are discouraged as all papers published must be able to stand on their own. Justification must be provided to the editor if an author feels as though the work must be presented in two parts and published simultaneously. There is no guarantee that companions will be reviewed by the same reviewers, which complicates the review process, increases the risk for rejection and potentially lengthens the review time. If this is a companion paper, please indicate the part number and provide the title, authors and manuscript number (if available) for the companion papers along with your detailed justification for the editor in the comments box below. If there is no justification provided, or if there is insufficient justification, the papers will be returned without review.	Ref.:Submittal of companion papers: “Physical Model Tests on Half-Scale Geosynthetic Reinforced Soil Bridge Abutments. I: Static Loading.” by Y. Zheng, P.J. Fox, P.B. Shing, and J.S. McCartney and “Physical Model Tests on Half-Scale Geosynthetic Reinforced Soil Bridge Abutments. II: Dynamic Loading.” by Y. Zheng, P.J. Fox, P.B. Shing, and J.S. McCartney for possible publication as Technical Papers in ASCE Journal of Geotechnical and Geoenvironmental Engineering Dear Editor, Please find enclosed our companion manuscripts submitted for review and possible publication as technical papers in Journal of Geotechnical and Geoenvironmental Engineering. The papers focus on physical model tests on geosynthetic reinforced soil (GRS) bridge abutments. We believe that the papers work well as a companion set because the first paper presents the experimental program and static response of GRS bridge abutments, while the second paper presents the dynamic response for a series of earthquake motions in the longitudinal direction. Please contact me should you need any clarification. I look forward to having this paper published in Journal of Geotechnical and Geoenvironmental Engineering. Best regards, Yewei Zheng
If this manuscript is intended as part of a Special Issue or Collection, please provide the Special Collection title and name of the guest editor in the comments box below.	
Recognizing that science and engineering are best served when data aremade available during the review and discussion of manuscripts andjournal articles, and to allow others to replicate and build on workpublished in ASCE journals, all reasonable requests by reviewers formaterials, data, and associated protocols must be fulfilled. If you are restricted from sharing your data and materials, please explain below.	
Papers published in ASCE Journals must make a contribution to the core body of	This paper presents experimental data on the dynamic response of half-scale GRS bridge abutments for a series of shaking table tests with scaled earthquake motions in

knowledge and to the advancement of the field. Authors must consider how their new knowledge and/or innovations add value to the state of the art and/or state of the practice. Please outline the specific contributions of this research in the comments box.	the longitudinal direction, including wall facing displacements, bridge seat settlements, accelerations, vertical and lateral soil stresses, reinforcement tensile strains, and bridge beam-bridge seat contact forces.
The flat fee for including color figures in print is $800, regardless of the number of color figures. There is no fee for online only color figures. If you decide to not print figures in color, please ensure that the color figures will also make sense when printed in black-and-white, and remove any reference to color in the text. Only one file is accepted for each figure. Do you intend to pay to include color figures in print? If yes, please indicate which figures in the comments box.	No
If there is anything else you wish to communicate to the editor of the journal, please do so in this box.	

Physical Model Tests of Half-Scale Geosynthetic Reinforced Soil Bridge Abutments. II: Dynamic Loading

Yewei Zheng, A.M.ASCE[1]; John S. McCartney, F.ASCE[2]; P. Benson Shing[3], M.ASCE; and Patrick J. Fox, F.ASCE[4]

Abstract: This paper presents experimental results from shaking table tests on four half-scale geosynthetic reinforced soil (GRS) bridge abutment specimens constructed using well-graded angular backfill sand, modular facing blocks, and uniaxial geogrid reinforcement to investigate the effects of applied surcharge stress, reinforcement vertical spacing, and reinforcement tensile stiffness for dynamic loading conditions. Similitude relationships for shaking table tests in a 1*g* gravitational field were used to scale the specimen geometry, applied surcharge stress, soil modulus, reinforcement tensile stiffness, and characteristics of the earthquake motions. Reinforcement vertical spacing and reinforcement tensile stiffness had the most significant effects on the maximum dynamic and residual wall facing displacements and bridge seat settlements. Acceleration amplification increased with elevation in the reinforced and retained soil zones. Residual vertical and lateral soil stresses were lower than the calculated values for static loading conditions. The maximum tensile strain in each reinforcement layer occurred near the facing block connection for lower layers and under the bridge seat for higher layers. The vertical seismic joint between the bridge beam and bridge seat closed during the Northridge motion, resulting in contact force. A companion paper presents experimental results for the same GRS bridge abutment specimens under static loading conditions.

Keywords: Geosynthetic reinforced soil; Bridge abutment; Retaining wall; Shaking table test; Dynamic loading.

---

[1] Assistant Professor, Department of Civil and Environmental Engineering, Old Dominion University, Norfolk, VA 23529 USA (corresponding author). ORCID: https://orcid.org/0000-0001-9038-4113. Email: y1zheng@odu.edu
[2] Professor and Chair, Department of Structural Engineering, University of California, San Diego, La Jolla, CA 92093-0085 USA. Email: mccartney@ucsd.edu
[3] Professor, Department of Structural Engineering, University of California, San Diego, La Jolla, CA 92093-0085 USA. Email: pshing@ucsd.edu
[4] Shaw Professor and Head, Department of Civil and Environmental Engineering, Pennsylvania State University, University Park, PA 16802 USA. Email: pjfox@engr.psu.edu

Introduction

Although geosynthetic reinforced soil (GRS) bridge abutments are commonly used for transportation applications, concerns remain regarding the performance of these structures in high seismicity areas and little information is available to guide designers on seismic response. A key concern for GRS bridge abutments is the magnitude of possible seismic-induced settlement (i.e., seismic compression) which, for example, could cause problematic loading for a multi-span bridge with intermediate supports. Associated wall facing displacements and other permanent deformations due to seismic shaking are also concerns, along with damage due to interactions between the bridge structure and abutments.

Numerical and experimental studies have been performed to investigate the static response of GRS bridge abutments; however, studies on the dynamic response of these structures are limited. Yen et al. (2011) conducted post-earthquake reconnaissance for the 2010 Maule earthquake and found that a GRS bridge abutment exhibited no signs of lateral or vertical permanent displacements after shaking, while the bridge suffered minor damage that may have resulted from the bridge skew angle. Shaking table tests have been conducted on GRS bridge abutments for shaking in both longitudinal and transverse directions to the bridge beam (Helwany et al. 2012; Zheng et al. 2018a, 2018b). Helwany et al. (2012) reported no significant distress for a 3.6 m-high GRS bridge abutment subjected to longitudinal shaking with horizontal base accelerations up to 1*g*. Zheng et al. (2018a, 2018b) conducted shaking table tests on 2.7 m-high half-scale GRS bridge abutments and found that facing displacements and bridge seat settlements were smaller for shaking in the longitudinal direction than in the transverse direction. Although these studies indicate good overall performance for GRS bridge abutments under dynamic loading, more experimental evaluations are needed to better understand the performance of these systems for various geometric configurations, reinforcement characteristics, and surcharge loading conditions.

This paper presents experimental results on the dynamic response of four half-scale GRS bridge abutment specimens constructed using well-graded backfill sand, modular facing blocks, and uniaxial geogrid reinforcement for a series of shaking table tests with scaled earthquake motions in the longitudinal direction. Wall facing displacements, bridge seat settlements, accelerations, soil stresses, reinforcement tensile strains, and bridge beam-bridge seat displacements and contact forces were measured to understand the effects of applied surcharge stress, reinforcement vertical spacing, and reinforcement tensile stiffness. A companion paper (Zheng et al. 2019) presents the static response of the same GRS bridge abutment specimens during construction and bridge loading.

Background

Past research studies have used shaking table tests to investigate the dynamic response of GRS walls (El-Emam and Bathurst 2004, 2005, 2007; Ling et al. 2005, 2012; Sabermahani et al. 2009; Guler and Enunlu 2009; Guler and Selek 2014; Fox et al. 2015; Latha and Santhanakumar 2015), with many of these tests conducted on reduced-scale models due to limitations of table size and payload capacity. Under such conditions, similitude relationships are required to yield a response that corresponds to the full-scale prototype structure. Iai (1989) proposed such relationships for shaking table tests on reduced-scale models in a 1*g* gravitational field, which have been widely used for studies on GRS structures (e.g., El-Emam and Bathurst 2004, 2005, 2007; Guler and Selek 2014; Latha and Santhanakumar 2015). El-Emam and Bathurst (2004, 2005, 2007) conducted a series of shaking table tests on 1 m-high, 1/6th-scale GRS walls subjected to sinusoidal motion with increasing amplitude at a frequency of 5 Hz, and found that facing displacements decreased with decreasing facing panel mass, increasing reinforcement length, increasing reinforcement stiffness, and decreasing reinforcement vertical spacing. Guler and Selek (2014) conducted a series of shaking table tests on model GRS walls with different scales and reported that accelerations were not affected by model scale and facing displacements for the prototype structure decreased with increasing model size. Latha and Santhanakumar (2015) found that higher relative density for the backfill soil significantly reduced lateral facing displacements and reinforced fill settlements during shaking table tests on 0.6 m-high, 1/8th-scale GRS walls.

Large-scale shaking table tests have also been conducted on GRS walls and abutments and are preferred when possible because materials and construction methods can more closely match field conditions. Ling et al. (2005, 2012) conducted such tests on 2.8 m-high modular block GRS walls using both sand and silty sand backfill soils. Results indicated that the walls had negligible deformations and horizontal acceleration amplification for a moderate earthquake motion (peak horizontal acceleration (PHA) = 0.40*g*), and relatively small deformations and horizontal acceleration amplification for a strong earthquake motion (PHA = 0.86*g*). Facing displacements decreased when reinforcement length for the top layer increased from 2.05 m to 2.52 m and reinforcement vertical spacing decreased from 0.6 m to 0.4 m. In addition, unsaturated conditions for the silty sand backfill soil were found to reduce dynamic facing displacements (Ling et al. 2012). Fox et al. (2015) conducted shaking table tests on a full-scale modular block GRS wall with a height of 6.1 m and reinforcement vertical spacing of 0.6 m. The wall experienced a maximum acceleration amplification of 2.41 for a 50% Northridge-Tarzana record. After a series of earthquake and sinusoidal motions, the wall had moderate damage, including a residual lateral facing displacement of 56 mm near the top, and the backfill soil exhibited two significant cracks with a width of more than 30 mm, one at the back of the reinforced soil zone and one near the rear boundary.

Helwany et al. (2012) conducted the first large-scale shaking table tests on a GRS bridge abutment with a height of 3.6 m using a series of horizontal sinusoidal motions with increasing amplitude in the longitudinal direction. The abutment specimen was constructed using poorly-graded gravel, modular block facing, and woven polypropylene geotextiles with a length of 2.8 m and vertical spacing of 0.2 m. For PHA = 0.67*g*, several blocks near the bottom corners of the abutment showed minor cracks and, at PHA = 1.0*g*, the abutment remained stable with some broken bottom corner blocks. The average incremental bridge seat settlement for PHA increasing from 0.67*g* to 1.0*g* was 48 mm (scaled from Figures 6.76 and 6.77 of Helwany et al. 2012), which corresponds to a vertical strain (i.e., settlement/height) for the lower GRS fill of 1.5%. Zheng et al. (2018a, 2018b) performed longitudinal and transverse shaking table tests on 2.7 m-high half-scale GRS bridge abutment specimens constructed using well-graded angular sand, modular facing blocks, and uniaxial geogrid layers with a vertical spacing of 0.15 m. The specimens were subjected to scaled motions from the 1940 Imperial Valley and 2010 Maule earthquakes with PHA = 0.31*g* and PHA = 0.40*g*, respectively. Zheng et al. (2018b) reported average incremental residual bridge seat settlements of 2.5 mm and 4.8 mm for the two scaled motions in the transverse shaking tests, which were larger than the corresponding measurement of 1.4 mm for each of the longitudinal shaking tests.

Experimental Program

The experimental program consisted of four GRS bridge abutment specimens, including a baseline case specimen (Specimen 1), a specimen with lower surcharge stress (Specimen 2), a specimen with larger reinforcement vertical spacing (Specimen 3), and a specimen with reduced reinforcement tensile stiffness (Specimen 4). Tests were conducted on the indoor uniaxial servo-hydraulic shaking table in the Charles Lee Powell Structural Research Laboratory at the University of California, San Diego (UCSD), which was refurbished prior to this study to increase the fidelity of dynamic motion (Trautner et al. 2017). Details regarding specimen configuration, material properties, construction procedures, and instrumentation are provided in the companion paper (Zheng et al. 2019). Other information relevant to the dynamic testing program is provided below.

Similitude Relationships

The Iai (1989) similitude relationships define three independent scaling factors for length, density, and strain to ensure a similar stress-strain response between model and prototype. The scaling factors for density and strain typically are assumed as unity for a given soil, leaving the length scaling factor as the main consideration. A length scaling factor of $\lambda = 2$, defined as the ratio of prototype length to specimen length, was used to design half-scale GRS bridge abutment specimens for the testing program. Corresponding scaling factors for specimen geometry, applied surcharge stress, soil modulus, reinforcement tensile stiffness, and characteristics of the earthquake motions are provided in Table 1.

Specimen Configuration

The configuration of the longitudinal shaking table tests is shown in Figures 1 and 2 of the companion paper (Zheng et al. 2019). A concrete beam represents a longitudinal slice of a prototype bridge structure and rests on a GRS bridge abutment with a concrete bridge seat at one end and on a concrete support wall at the other end. Elastomeric bearing pads were placed under both ends of the bridge beam, with properties reported by Zheng et al. (2018a). Each GRS bridge abutment specimen has modular block facing on three sides, including a front wall and two side walls, and a back side supported by a rigid reaction wall consisting of a steel frame with plywood facing. The reaction wall was designed to be sufficiently stiff to maintain at-rest lateral earth pressures during construction and experience minimal deflections during shaking (Zheng 2017; Zheng et al. 2018a). Considering that the reaction wall does not reproduce a deformation boundary condition consistent with a retained soil mass in the field, the thickness of the retained soil zone (0.63 m) was maximized within the geometry and payload constraints of the table. The base of the concrete support wall is rigidly connected to the shaking table with steel beams to transmit table motions and includes a sliding platform designed using the low-friction boundary concept of Fox et al. (1997, 2006). Zheng et al. (2018a) evaluated the performance of the testing system and found that the shaking table was able to reproduce the salient characteristics of the scaled earthquake motions, the reaction wall moved in phase with the shaking table, and the steel connection beams and sliding platform successfully transmitted table motions to the base of the support wall.

With a length scaling factor of $\lambda = 2$, the GRS bridge abutment specimens correspond to a prototype structure with a total height of 5.4 m and a bridge clearance height of 4.5 m. This clearance height meets Federal Highway Administration (FHWA) requirements (Stein and Neuman 2007). For Specimens 1, 3, and 4, the average applied surcharge stress on the backfill soil from the bridge seat due to the total weight of bridge seat, bridge beam, and dead weights is 66 kPa. This corresponds to a prototype surcharge stress of 132 kPa and is in the typical range for GRS bridge abutments in the field (Adams et al. 2011). Specimen 2 was tested with a lower weight of bridge beam, which yields an applied surcharge stress of 43 kPa and a prototype surcharge stress of 86 kPa. The width of the vertical seismic joint between the bridge beam and back wall of the bridge seat is 25 mm. During shaking, the bridge beam interacts with the GRS bridge abutment and support wall through friction developed at the bearing pads and the bridge beam may potentially contact with the back wall of the bridge seat due to sliding.

Soil and Reinforcement

The half-scale bridge abutment specimens were constructed using a clean well-graded angular sand, consisting primarily of crushed rock, with no gravel and a low fines content. A summary of soil properties is provided in Table 2 of the companion paper (Zheng et al. 2019). Based on the standard Proctor test, the sand has a maximum dry unit weight of 18.4 kN/m^3 and optimum gravimetric water content of 11.4%. A target gravimetric water content of 5% was selected for construction to minimize dust and loss of fines during soil placement and compaction. A relative density D_r = 85% was chosen for the prototype abutment structure, which corresponds to a relative compaction of 96% and meets field compaction requirements for GRS bridge abutments (Berg et al. 2009; Adams et al. 2011). Once the prototype relative density was established, consolidated-drained (CD) triaxial compression tests were conducted to determine the target relative density for construction of the half-scale GRS abutment specimens.

Measured relationships for stress ratio σ_1'/σ_3' versus axial strain from five CD triaxial tests on dry sand specimens are shown in Figure 1. An initial test was conducted for D_r = 85% (initial void ratio e_o = 0.443) and effective confining stress σ_3' = 69.0 kPa to provide the average stress-strain response of the backfill soil at the mid-height of a prototype structure. Using the stress scaling factor (= 2) in Table 1, four additional CD triaxial tests were conducted for σ_3' = 34.5 kPa and D_r = 45%, 60%, 70%, and 85%. The relationship for D_r = 70% and σ_3' = 34.5 kPa yielded similar stiffness and strength to that for the prototype and, as such, a value of D_r = 70% was chosen for construction the half-scale abutment specimens. The corresponding density ratio for the 85%/69.0 kPa and 70%/34.5 kPa specimens is 1.05 (= 1808 kg/m^3/1722 kg/m^3) and the strain ratio at peak is 0.87 (= 5.05%/5.79%), which are small deviations from the theoretical values of unity in Table 1.

A uniaxial high-density polyethylene (HDPE) geogrid was used to construct the half-scale abutment specimens. Specimens 1 and 2 had intact reinforcement layers with a vertical spacing S_v = 0.15 m, Specimen 3 had intact reinforcement layers with S_v = 0.3 m, and Specimen 4 had reduced stiffness/strength reinforcement layers (i.e., every other geogrid rib in the transverse direction removed) with S_v = 0.15 m. Using the scaling factor in Table 1, the geogrid tensile stiffness at 5% strain ($J_{5\%}$) = 380 kN/m and geogrid tensile strength (T_{ult}) = 38 kN/m for Specimens 1, 2, and 3 correspond to 1520 kN/m and 152 kN/m, respectively, for a prototype geogrid, which are typical values for field applications. Corresponding prototype values for Specimen 4 are $J_{5\%}$ = 760 kN/m and T_{ult} = 76 kN/m. Tensile tests were conducted on single rib geogrid specimens for average strain rates of 1, 5, 10, 50, and 100%/min. according to ASTM D6637. Results of these tests are presented in Figure 2 and indicate that tensile stiffness and strength increase with increasing strain rate.

Instrumentation

Experimental data were collected using an automatic data acquisition system with 160 channels at a sampling rate of 256 Hz. Sensor details are provided by Zheng et al. (2018a). Instrumentation layouts for the longitudinal centerline section L1, located at distance y = 0.8 m from the west side wall facing, longitudinal off-centerline section L2, located at y = 0.35 m, and transverse section T1 under the bridge seat, located at distance x = 0.48 m from the front wall facing, are shown in Figure 7 of the companion paper (Zheng et al. 2019).

Input Motions

The GRS bridge abutment specimens were shaken in the longitudinal direction using three consecutively-applied scaled earthquake motions, as summarized in Table 2, with low-acceleration white noise motion applied in between each earthquake motion (Zheng 2017). As such, initial conditions (e.g., stiffness) likely were different for each abutment specimen prior to each earthquake motion due to residual plastic deformations from previous shaking events. Consecutive application of earthquake motions allowed more information to be obtained from each abutment specimen, and has been used for other shaking table testing programs (Ling et al. 2005, 2012; and Fox et al. 2015).

The earthquake motions were applied in displacement-control mode and scaled from original records of the 1940 Imperial Valley earthquake (El Centro station), 2010 Maule earthquake (Concepcion station), and 1994 Northridge earthquake (Newhall station), all of which were obtained from the Pacific Earthquake Engineering Research Center (PEER) Ground Motion Database (https://ngawest2.berkeley.edu/). Acceleration and displacement time histories for the original and scaled Imperial Valley motions are shown in Figure 3. The original motion has PHA = 0.31*g*, peak horizontal velocity (PHV) = 296.9 mm/s, and peak horizontal displacement (PHD) = 130.4 mm. The scaled acceleration time history was obtained by maintaining acceleration amplitudes and increasing acceleration frequencies by a factor of $\sqrt{2}$ (Table 1), and the scaled displacement time history was obtained by double integration of the scaled acceleration time history. Resulting target values for PHA, PHV, and PHD for the scaled earthquake motions are provided in Table 2. Actual values of PHA measured from the shaking table range from 0.41*g* to 0.46*g* for the Imperial Valley motion, 0.52*g* to 0.58*g* for the Maule motion, and 0.98*g* to 1.09*g* for the Northridge motion. Although the measured PHA values exceed the target values for each specimen and scaled earthquake motion, comparisons of the pseudo-acceleration response spectra indicate that the response of the shaking table is in close agreement with the target motion for frequencies up to approximately 6 Hz (Zheng 2017; Zheng et al. 2018a).

Experimental Results

Experimental results are presented for four GRS bridge abutment specimens and three instrumented sections (L1, L2, and T1) for each specimen to evaluate dynamic response, including wall facing displacements, bridge seat settlements, accelerations, soil stresses, reinforcement tensile strains, and bridge beam-bridge seat displacements and contact forces. Partial results for Specimen 1 are presented by Zheng et al. (2018a) and complete results, including time histories, are provided by McCartney et al. (2018). Horizontal displacements and accelerations toward the north, outward displacements for the front wall and side wall facings, and downward displacements (i.e., settlements) for the bridge seat are defined as positive. Maximum profiles for facing displacements, soil stresses, and reinforcement tensile strains present the highest measured value for each individual sensor during the shaking event, and thus do not correspond to a single point in time, and residual profiles present final values after shaking. The presented results are measured values and must be adjusted using the scaling factors in Table 1 to obtain corresponding values for a prototype structure.

Facing Displacements

Profiles of incremental maximum wall facing displacement and incremental residual wall facing displacement for the four abutment specimens and the Imperial Valley motion are compared in Figure 4, with all values taken relative to initial facing displacements before the start of the shaking event. The profiles display similar trends with displacements generally increasing with elevation and highest values measured near or at the top of each wall. Maximum values during shaking were substantially recovered after shaking was completed, especially in the upper section of the walls.

Measurements for the front wall in longitudinal centerline section L1 are shown in Figure 4(a) and indicate that Specimens 3 and 4 had significantly larger incremental maximum and residual facing displacements near the top than Specimen 1. This indicates the importance of reinforcement vertical spacing and reinforcement tensile stiffness with regard to facing displacements for dynamic loading, and is consistent with similar observations for static loading in the companion paper (Zheng et al. 2019). Specimen 3 yielded the highest values of 7.2 mm (maximum) and 4.4 mm (residual) at the top of the wall, which correspond to 14.4 mm and 8.8 mm for a prototype structure. Maximum facing displacements for Specimen 1 were larger than Specimen 2 for the upper half of the wall; however, Specimen 1 experienced smaller residual displacements. Profiles for the front wall in longitudinal off-centerline section L2 are presented in Figure 4(b) and show similar trends. Displacement magnitudes were smaller than for L1, with highest incremental displacements of 6.1 mm (maximum) and 3.2 mm (residual) again measured for Specimen 3 at the top of the wall. Profiles for the west side wall in transverse section T1 are shown in Figure 4(c) and display smoother, more linear relationships with highest values consistently measured at the top of the wall. In this case, Specimen 2 yielded the largest maximum displacements and Specimen 3 yielded the largest residual displacements. After shaking, residual values for Specimens 1 and 2 were similar and smaller than for Specimens 3 and 4, which again highlights the importance of reinforcement vertical spacing and reinforcement tensile stiffness.

The highest values of incremental maximum and incremental residual facing displacement for each abutment specimen, cross section, and scaled earthquake motion are compared in Figure 5. The data indicate clear trends, and some variability that may be attributed to differences in specimen construction and characteristics of the scaled motions. First considering the front wall, maximum values were similar for longitudinal sections L1 and L2 and increased with increasing PHA, larger reinforcement vertical spacing, and reduced reinforcement tensile stiffness. Consistent with Figures 4(a) and 4(b), Specimen 3 yielded the largest displacement values. Interestingly, with the exception of the Imperial Valley motion, maximum facing displacements were larger for Specimen 2 than for Specimen 1 even though the bridge beam had lower inertial mass for Specimen 2. This is in contrast to observations for static loading (Zheng et al. 2019) and attributed to the lower applied surcharge stress and associated lower soil stiffness for Specimen 2. Residual displacements for sections L1 and L2 were substantially smaller in all cases and show similar trends. Displacements for the west side wall in transverse section T1 indicate some differences relative to the longitudinal sections; the Maule motion produced the lowest values, reinforcement vertical spacing and reinforcement tensile stiffness show a less significant effect than for the longitudinal sections, and residual displacements were considerably smaller relative to maximum values. The results in Figures 4 and 5 also show that shaking in the longitudinal direction produced significant facing displacements for the side walls in the transverse direction, which indicates multi-directional deformation response of the abutment specimens.

Bridge Seat Settlements

Time histories of incremental bridge seat settlement for the abutment specimens during the Imperial Valley motion, taken as the average of measurements at the four top corners of each bridge seat, are shown in Figure 6. For Specimen 1, the maximum settlement was 3.1 mm and the minimum settlement was -0.1 mm (i.e., heave) during shaking, and the residual settlement after shaking was 1.4 mm, which yields an incremental residual vertical strain of 0.07% for the 2.1 m-high lower GRS fill. This residual settlement corresponds to 2.8 mm for the prototype, which is unlikely to be a concern for field applications. Consistent with front wall facing displacements (Figure 4), the largest values of maximum settlement (6.3 mm, 0.30%) and residual settlement (5.5 mm, 0.26%) were recorded for Specimen 3.

Incremental residual bridge seat settlements for each abutment specimen and scaled earthquake motion are compared in Figure 7, with values from Stage 3 static loading (i.e., bridge beam placement) also included from the companion paper (Zheng et al. 2019). For static loading, settlements range from 1.5 mm to 3.5 mm and, relative to Specimen 1, decreased with lower surcharge stress, increased with larger reinforcement vertical spacing, and increased slightly with reduced reinforcement tensile stiffness. After shaking, the trends are more pronounced with values ranging from 1.4 mm to 7.2 mm. Residual settlements increased with increasing PHA and show the same effects for reinforcement spacing and stiffness; however, lower surcharge stress produced larger settlements due to lower soil stiffness and generally larger wall facing displacements (and presumably soil shear strains) for Specimen 2 relative to Specimen 1 (Figure 5). Figures 5 and 7 indicate that larger residual bridge seat settlements generally occurred with larger residual wall facing displacements, although the values are not proportional and the trend is more consistent for front wall displacements (L1, L2) than side wall displacements (T1).

Accelerations

The root-mean-square (RMS) acceleration can be used to quantify the intensity of motion at a specific sensor or location and mitigate the effect of large, high-frequency acceleration spikes (or noise) that would skew an analysis based on maximum acceleration values alone (Kramer 1996; El-Emam and Bathurst 2005). RMS acceleration is calculated as the square root of the duration-normalized area under the record of (acceleration)^2 versus time, and captures the effects of amplitude, frequency content, and duration on dynamic response.

Vertical profiles of RMS acceleration ratio within the reinforced soil zone (x = 0.48 m) and retained soil zone (x = 1.78 m) for Specimen 1 are shown in Figure 8, where values are equal to the RMS acceleration measured in the longitudinal direction at a given sensor divided by the corresponding RMS acceleration measured at the shaking table. For the reinforced soil zone in Figure 8(a), ratios increased approximately linearly with elevation for sections L1 and L2 and all three scaled earthquake motions. Values were nearly equal for the Maule and Northridge motions and significantly higher for the Imperial Valley motion. The Imperial Valley motion yielded the maximum ratio of 1.57, which occurred for section L1 at the top of the reinforced soil zone and indicates significant amplification within the abutment specimen. Differences in RMS acceleration ratio for the scaled motions are attributed to differences in motion characteristics, such as frequency content, as well as differences in response characteristics of Specimen 1, such as stiffness, which may have been influenced by prior shaking events. Corresponding measurements for the retained soil zone are shown in Figure 8(b) and display similar trends. RMS acceleration ratio profiles for sections L1 and L2 were consistently in close agreement for each soil zone.

Vertical profiles of RMS acceleration ratio within the reinforced soil zone (x = 0.48 m) and retained soil zone (x = 1.78 m) in longitudinal section L1 for each abutment specimen and the

Imperial Valley motion are presented in Figure 9. Again, the plots show similar values and trends for the two soil zones, with values increasing with elevation in all cases. At any given elevation, ratios were lowest and nearly equal for larger reinforcement vertical spacing (Specimen 3) and reduced reinforcement tensile stiffness (Specimen 4), higher for lower surcharge stress and inertial mass of the bridge beam (Specimen 2), and highest for the baseline case (Specimen 1). These findings differ from results reported by El-Emam and Bathurst (2007), in which, beyond a critical acceleration, acceleration amplification for GRS walls increased with larger reinforcement vertical spacing and reduced reinforcement tensile stiffness, and thus illustrate that system dynamic response can vary significantly from one study to the next depending on input motion and structure characteristics.

RMS acceleration ratios measured for specimen bridge seats and bridge beams during the three scaled earthquake motions are presented in Figure 10, where measurement locations are indicated in Figure 7a of the companion paper (Zheng et al. 2019). For each abutment specimen, ratios for the bridge seat were similar to ratios near the top of the reinforced soil zone (Figures 8a and 9a) and smaller than ratios for the bridge beam. This indicates that each bridge seat moved with the lower GRS fill and the bridge beam experienced even larger amplification. The highest ratio for each motion occurred for the bridge beam with lowest inertial mass (Specimen 2). Similar to the reinforced and retained soil zones (Figure 8), RMS acceleration ratios for the bridge seats and bridge beams for the Imperial Valley motion were higher than corresponding ratios for the Maule and the Northridge motions.

Soil Stresses

Vertical and lateral soil stresses were measured using load cell-based, contact earth pressure cells with capacities of 160 kPa and 320 kPa. This type of pressure cell does not require special correction for dynamic testing and has been used successfully for previous investigations of static and dynamic soil-structure interaction (e.g., Fox et al. 2015; Keykhosropour et al. 2018). Profiles of vertical soil stress behind the front wall facing for section L1 of each abutment specimen during and after the Imperial Valley motion are presented in Figure 11. Maximum values during shaking, shown in Figure 11(a), display similar trends and higher magnitudes relative to final values for static loading (Figure 13b, Zheng et al. 2019), and indicate an approximately trapezoidal distribution for Specimens 2, 3, and 4, and a high value (103.9 kPa) at the top for Specimen 1. Calculated values from the AASHTO (2012) method for static loading (Stage 3), according to a 2:1 distribution for surcharge stress, are also shown in Figure 11(a) and were generally close to the maximum stresses during shaking, except at the top for Specimen 1. Profiles of incremental maximum vertical stress, taken relative to the final values for static loading, are shown in Figure 11(b). Overall, incremental stresses were approximately constant with elevation, with highest values occurring for larger reinforcement vertical spacing (Specimen 3). Corresponding plots of residual vertical stress are shown in Figure 11(c). After shaking, measured residual stresses were smaller than the AASHTO (2012) values except at the top for Specimen 1. Incremental residual vertical stress profiles, also taken relative to final values for static loading, are shown in Figure 11(d) and display more consistent trends. Interestingly, vertical stresses significantly increased due to shaking, with incremental profiles approximately trapezoidal for Specimen 1 and triangular for the other specimens. The increase in vertical stress is attributed to loss of support of the weight of backfill soil from friction on the facing blocks and horizontal reinforcement layers near the front wall facing (e.g., Runser et al. 2001), and a resulting redistribution of vertical soil stress. The abutment specimens also experienced small increases in residual vertical stress for the other scaled earthquake motions (not shown), with magnitudes increasing toward the base and highest values ranging from 5 kPa to 20 kPa (McCartney et al. 2018).

Lateral soil stresses behind the front wall facing are presented in Figure 12, along with calculated values from the AASHTO (2012) method for static loading. To obtain the calculated values, the AASHTO (2012) vertical stress profiles in Figure 11 were multiplied by the Rankine active earth pressure coefficient K_a (= 0.12). In Figure 12(a), maximum lateral stresses during shaking generally were larger near the top and bottom than at mid-height for Specimens 1 and 2 and larger at the bottom for Specimens 3 and 4, with the highest value of 13 kPa at the top of the wall (Specimen 2). Most of the measurements were smaller than AASHTO (2012) calculated values for static loading. In Figure 12 (b), values of incremental maximum stress range from 1 to 8 kPa, and overall are approximately constant with elevation and show no clear trend with regard to specimen type. Profiles of measured residual lateral stress, shown in Figure 12(c), generally decreased with increasing elevation and again generally were lower than AASHTO (2012) calculated values. In Figure 12(d), the incremental residual stress profiles are approximately constant with elevation and display generally higher values for larger reinforcement vertical spacing (Specimen 3) and highest values for reduced reinforcement tensile stiffness (Specimen 4). Figure 12(d) also indicates that residual lateral stresses increased due to shaking, in part due to associated increases in vertical stress shown in Figure 11(d), such as for Specimens 3 and 4 at the bottom of the wall. The abutment specimens also experienced similar small increases in residual lateral stress for the other scaled earthquake motions (not shown), with magnitudes approximately constant with elevation and highest values ranging from 1 kPa to 6 kPa (McCartney et al. 2018).

Reinforcement Strains

Distributions of measured residual tensile strain in reinforcement layers for the three instrumented sections of Specimen 1 after Stage 3 static loading (Zheng et al. 2019) and each scaled earthquake motion are presented in Figure 13. Zero strain at the free end of each reinforcement layer is also plotted. Tensile strains for longitudinal section L1, shown in Figure 13(a), progressively increased under the bridge seat due to successive shaking events. For instance, the strain at x = 0.45 m in geogrid layer 10 was 0.11% after Stage 3, and then increased to 0.16% after Imperial Valley, 0.20% after Maule, and 0.27% after Northridge. Tensile strains near the facing block connections (x = 0.10 m) increased only for layer 1, and experienced slight decreases in higher layers, which is attributed to loosening of backfill soil near the connections due to the inertial forces of facing blocks during shaking. Tensile strains for longitudinal section L2, shown in Figure 13(b), were similar to values for section L1 in layers 1 and 7 and much higher in layer 13 under the bridge seat. This is attributed to tilting of the bridge seat toward the west side (section L2) during placement of the bridge beam (Figure 12, Zheng et al. 2019) and possibly subsequent higher surcharge stress on that side during shaking. In Figure 13(c), strains for transverse section T1 increased progressively near the connection in layer 1 and under the bridge seat in higher layers. The data indicate that shaking in the longitudinal direction produced tensile strains in transverse reinforcement layers, which is consistent with the results for side wall facing displacements in Figures 4 and 5.

Plots of incremental maximum and incremental residual tensile strain, taken relative to initial strains before shaking, are shown in Figure 14 for sections L1 and T1 of each abutment specimen and the Imperial Valley motion. Although some variability is observed, maximum strains in Figure 14(a) and Figure 14(b) generally increased with lower surcharge stress, larger reinforcement vertical spacing, and reduced reinforcement tensile stiffness. Similar to Figure 13, these strain increases were most significant for lower reinforcement layers at the facing connections and for higher reinforcement layers under the bridge seat. The effect can be significant as observed, for example, the incremental maximum strain increased from 0.09% to 0.33% under the bridge seat for layer 13 in section L1, when the reinforcement vertical spacing was increased from 0.15 m (Specimen 1) to 0.3 m (Specimen 3). Corresponding plots for incremental residual strains in Figure 14(c) and Figure 14(d) show similar trends and significant additional strains, as high as 0.21%, for the reinforcement as a result of the shaking event.

Bridge Seat and Bridge Beam Interaction

Horizontal displacements were measured in the longitudinal direction for the bridge beam and two bottom corners of the bridge seat for each abutment specimen (Zheng et al. 2019). Incremental displacement time histories for Specimen 1 during the Northridge motion are shown in Figure 15(a). Displacements at the east and west sides of the bridge seat were similar with respect to both trend and magnitude, which indicates nearly uniform translational movement of the bridge seat in the longitudinal direction during shaking. The bridge beam also shows a similar displacement trend and much larger magnitudes than the bridge seat, which indicates sliding of the bridge beam relative to the bridge seat on the bearing pad interface. The time history of bridge beam displacement relative to average bridge seat displacement is shown in Figure 15(b). During shaking, the bridge beam experienced maximum relative displacements of 20.6 mm toward the north and 30.0 mm toward the south and had a residual relative displacement of 4.3 mm toward the south after shaking. The vertical seismic joint closed and contact occurred between the bridge beam and bridge seat at t = 4.0 s and, after shaking, remained open with a residual width of 25.7

mm. The horizontal contact force was measured using two load cells embedded in the south end of the bridge beam (Figure 7, Zheng et al. 2019) and is plotted in Figure 16. The tips of the load cells made contact at slightly different times and with different force magnitudes. For all specimens and shaking events, contact occurred only during the Northridge motion. Maximum contact forces were taken as the peak of the time-synchronized sum of measurements from the two load cells in each case and equal to 98.5 kN, 110.3 kN, 68.5 kN, and 105.2 kN for Specimens 1, 2, 3, and 4, respectively. Interestingly, the highest contact force occurred for Specimen 2, which had the highest acceleration ratio (Figure 10) and lowest bridge beam inertial mass.

Conclusions

This paper presents experimental results from shaking table tests on four half-scale geosynthetic reinforced soil (GRS) bridge abutment specimens constructed using well-graded backfill sand, modular facing blocks, and uniaxial geogrid reinforcement. The specimens included a baseline case (Specimen 1), lower surcharge stress (Specimen 2), larger reinforcement vertical spacing (Specimen 3), and reduced reinforcement tensile stiffness (Specimen 4). Results are presented for a series of scaled earthquake motions in the longitudinal direction. The following conclusions are reached for the conditions of the study:

1. The abutment specimens experienced similar profiles of wall facing displacement, with displacements generally increasing with elevation and highest values measured near or at the top of each wall. Maximum values during shaking were substantially recovered after shaking, especially in the upper section of the walls. For the front walls, incremental maximum and incremental residual facing displacements generally increased with increasing peak horizontal acceleration (PHA), larger reinforcement vertical spacing,

reduced reinforcement stiffness, and lower surcharge stress. Shaking in the longitudinal direction produced significant facing displacements for the side walls in the transverse direction, which indicates multi-directional deformation response of the abutment specimens.

2. Residual bridge seat settlements increased with increasing PHA, larger reinforcement vertical spacing, reduced reinforcement stiffness, and lower surcharge stress. Larger residual bridge seat settlements generally were associated with larger residual wall facing displacements.
3. Root-mean-square (RMS) acceleration ratio in the reinforced and retained soil zones increased approximately linearly with elevation for each abutment specimen, and decreased with larger reinforcement vertical spacing, reduced reinforcement tensile stiffness, and lower surcharge stress and inertial mass of the bridge beam. RMS acceleration ratios indicate that each bridge seat moved with the lower GRS fill and each bridge beam experienced even larger amplification.
4. Measured values of maximum vertical and maximum lateral soil stresses behind the front wall facing during shaking generally were close to or smaller than values calculated using the AASHTO (2012) method for static loading. Residual vertical and lateral soil stresses generally were smaller than AASHTO (2012) calculated values for static loading, and increased due to shaking, which is attributed to loss of support of the weight of backfill soil near the front wall facing.
5. For successive shaking events, tensile strains increased near the facing block connections for lower reinforcement layers and under the bridge seat for higher reinforcement layers. Consistent with incremental facing displacements, incremental tensile strains increased

with larger reinforcement vertical spacing, reduced reinforcement stiffness, and lower surcharge stress.

6. Each bridge beam experienced sliding relative to the bridge seat during shaking and permanent displacement afterward. The vertical seismic joint closed during the Northridge motion for each abutment specimen, resulting in contact force between the bridge beam and bridge seat. The highest contact force occurred for Specimen 2 with the highest bridge beam RMS acceleration ratio and lowest bridge beam inertial mass.

The GRS bridge abutment specimens in the current study were limited by the size and payload capacity of the shaking table. Field GRS bridge abutments have a larger retained soil mass behind the reinforced soil zone, which may potentially increase abutment deformations. In addition, widths of the abutment specimens in the transverse direction proportionally were smaller than for field structures, which may have produced some differences in dynamic response. The overlap of geogrid reinforcement in the transverse and longitudinal directions across the entire reinforced soil zone may have produced a relatively stiff response for the half-scale abutment specimens, as such overlap would be limited to the corners for a typical GRS bridge abutment in the field.

Acknowledgements

Financial support for this study provided by the California Department of Transportation (Caltrans) Project 65A0556 with Federal Highway Administration (FHWA) Pooled Fund Project 1892AEA is gratefully acknowledged. The authors thank Dr. Charles Sikorsky and Kathryn Griswell of Caltrans for their support and assistance with the project. The first author gratefully acknowledges a GSI Fellowship provided by the Geosynthetic Institute. The authors also thank the staff and undergraduate research assistants at the UCSD Powell Structural Laboratories for their help with the experimental work. The geogrid used in this study was provided by the Tensar International Corporation, Inc.

Notation

The following symbols are used in this paper:

D_r = relative density

e_0 = initial void ratio

$J_{5\%}$ = secant stiffness of reinforcement at 5% tensile strain

K_a = Rankine coefficient of active earth pressure

S_v = reinforcement vertical spacing

t = time

T_{ult} = ultimate strength of reinforcement

x = distance from front wall facing

y = distance from west side wall facing

z = elevation above foundation soil

λ = scaling factor

σ_1' = major principal effective stress

σ_3' = minor principal effective stress

References

AASHTO. (2012). *AASHTO LRFD bridge design specifications*, 6th Edition, American Association of State Highway and Transportation Officials, Washington, D.C.

Adams, M., Nicks, J., Stabile, T., Wu, J., Schlatter, W., and Hartmann, J. (2011). “Geosynthetic reinforced soil integrated bridge system interim implementation guide.” *FHWA-HRT-11-026*, U.S. DOT, Washington, D.C.

ASTM D6637-15, *Standard Test Method for Determining Tensile Properties of Geogrids by the Single or Multi-Rib Tensile Method*, ASTM International.

Berg, R.R., Christopher, B.R., and Samtani, N. (2009). “Design and construction of mechanically stabilized earth walls and reinforced soil slopes – Volume I.” *FHWA-NHI-10-024*, U.S. DOT, Washington, D.C.

El-Emam, M., and Bathurst, R.J. (2004). “Experimental design, instrumentation and interpretation of reinforced soil wall response using a shaking table.” *International Journal of Physical Modelling in Geotechnics*, 4(4), 13-32.

El-Emam, M., and Bathurst, R.J. (2005). “Facing contribution to seismic response of reduced-scale reinforced soil walls.” *Geosynthetics International*, 12(5), 215-238.

El-Emam, M., and Bathurst, R.J. (2007). “Influence of reinforcement parameters on the seismic response of reduced-scale reinforced soil retaining walls.” *Geotextiles and Geomembranes*, 25(1), 33-49.

Fox, P.J., Andrew, A.C., Elgamal, A., Greco, P., Isaacs, D., Stone, M., and Wong, S. (2015). “Large soil confinement box for seismic performance testing of geo-structures.” *Geotechnical Testing Journal*, 38(1), 72-84.

Fox, P.J., Rowland, M.G., Scheithe, J.R., Davis, K.L., Supple, M.R., and Crow, C.C. (1997). "Design and evaluation of a large direct shear machine for geosynthetic clay liners." *Geotechnical Testing Journal*, 20(3), 279-288.

Fox, P.J., Nye, C.J., Morrison, T.C., Hunter, J.G., and Olsta, J.T. (2006). "Large dynamic direct shear machine for geosynthetic clay liners." *Geotechnical Testing Journal*, 29(5), 392-400.

Guler, E., and Enunlu, A.K. (2009). "Investigation of dynamic behavior of geosynthetic reinforced soil retaining structures under earthquake loads." *Bulletin of Earthquake Engineering*, 7(3), 737-777.

Guler, E., and Selek, O. (2014). "Reduced-scale shaking table tests on geosynthetic-reinforced soil walls with modular facing." *Journal of Geotechnical and Geoenvironmental Engineering*, 10.1061/(ASCE)GT.1943-5606.0001102, 04014015.

Helwany, S.M.B., Wu, J.T.H., and Meinholz, P. (2012). Seismic design of geosynthetic-reinforced soil bridge abutments with modular block facing. *NCHRP Web-Only Document 187*, Transportation Research Board, Washington, D.C.

Iai, S. (1989). "Similitude for shaking table tests on soil-structure-fluid models in 1 g gravitational fields." *Soils and Foundations*, 29(1), 105-118.

Keykhosropour, L., Lemnitzer, A., Star, L., Marinucci, A., and Keowen, S. (2018). "Implementation of soil pressure sensors in large-scale soil-structure interaction studies," Geotechnical Testing Journal, 41(4), 730–746.

Kramer, S.L. (1996). *Geotechnical Earthquake Engineering*, Prentice Hall, Upper Saddle River, NJ. 653pp.

Latha, G.M., and Santhanakumar, P. (2015). “Seismic response of reduced-scale modular block and rigid faced reinforced walls through shaking table tests.” *Geotextiles and Geomembranes*, 43(4), 307-316.

Ling, H.I., Mohri, Y., Leshchinsky, D., Burke, C., Matsushima, K., and Liu, H. (2005). “Large scale shaking table tests on modular block reinforced soil retaining wall.” *Journal of Geotechnical and Geoenvironmental Engineering*, 131(4), 465-476.

Ling, H.I., Leshchinsky, D., Mohri, Y., and Wang, J. (2012). “Earthquake response of reinforced segmental retaining walls backfilled with substantial percentage of fines.” *Journal of Geotechnical and Geoenvironmental Engineering*, 138(8), 934-944.

McCartney, J.S., Shing, P.B., Zheng, Y., Rong, W., and Fox, P.J. (2018). “Interaction of MSE abutments with bridge superstructures under seismic loading – shaking table tests.” *Report No. SSRP 18-01*, California Department of Transportation (Caltrans), Sacramento, CA, USA.

Runser, D., Fox, P. J., and Bourdeau, P.L. (2001). “Field performance of a 17 m-high reinforced soil retaining wall.” *Geosynthetics International*, 8(5), 367-391.

Sabermahani, M., Ghalandarzadeh, A., and Fakher, A. (2009). “Experimental study on seismic deformation modes of reinforced-soil walls.” *Geotextiles and Geomembranes*, 27(2), 121-136.

Stein, W. J., and Neuman, T. R. (2007). *Mitigation strategies for design exceptions*. FHWA-SA-07-011, U.S. DOT, Washington, D.C.

Trautner, C.A., Zheng, Y., McCartney, J.S., and Hutchinson, T.C. (2017). “An approach for shake table performance evaluation during repair and retrofit actions.” *Earthquake Engineering and Structural Dynamics*, 10.1002/eqe.2942.

Yen, W.-H.P., Chen, G., Buckle, I., Allen, T., Alzamora, D., Ger, J., and Arias, J.G. (2011). Post-earthquake reconnaissance report on transportation infrastructure: Impact of the February 27, 2010, offshore Maule Earthquake in Chile, *FHWA-HRT-11-030*, U.S. DOT, Washington, D.C.

Zheng, Y. (2017). Numerical simulations and shaking table tests of geosynthetic reinforced soil bridge abutments. *Ph.D. Dissertation*, University of California, San Diego, La Jolla, CA.

Zheng, Y., Sander, A.C., Rong, W., Fox, P.J., Shing, P.B., and McCartney, J.S. (2018a) "Shaking table test of a half-scale geosynthetic-reinforced soil bridge abutment." *Geotechnical Testing Journal*, 10.1520/GTJ20160268.

Zheng, Y., McCartney, J.S., Shing, P.B., and Fox, P.J. (2018b). "Transverse shaking table test of a half-scale geosynthetic reinforced soil bridge abutment." *Geosynthetics International*, DOI: 10.1680/jgein.18.00019.

Zheng, Y., Fox, P.J., Shing, P.B., and McCartney, J.S. (2019). "Physical model tests of half-scale geosynthetic reinforced soil bridge abutments. I: Static loading." *Journal of Geotechnical and Geoenvironmental Engineering* (companion paper, in review).

Table 1. Similitude relationships for 1*g* shaking table tests (Iai 1989).

Variable	Theoretical scaling factor	Scaling factor for λ = 2
Length	λ	2
Density	1	1
Strain	1	1
Mass	λ^3	8
Acceleration	1	1
Velocity	$\lambda^{1/2}$	1.414
Stress	λ	2
Modulus	λ	2
Stiffness	λ^2	4
Force	λ^3	8
Time	$\lambda^{1/2}$	1.414
Frequency	$\lambda^{-1/2}$	0.707

Table 2. Scaled earthquake motions for shaking table tests.

Scaled earthquake motion	Duration (s)	Target PHA (*g*)	Actual PHA (*g*)	Target PHV (mm/s)	Actual PHV (mm/s)	Target PHD (mm)	Actual PHD (mm)
Imperial Valley	28.3	0.31	0.41-0.46	209.9	214.5-224.5	65.2	64.7-65.2
Maule	100.4	0.40	0.52-0.58	415.7	427.6-429.8	108.0	107.7-108.0
Northridge	28.3	0.58	0.98-1.09	529.0	492.3-495.6	88.7	88.5-88.7

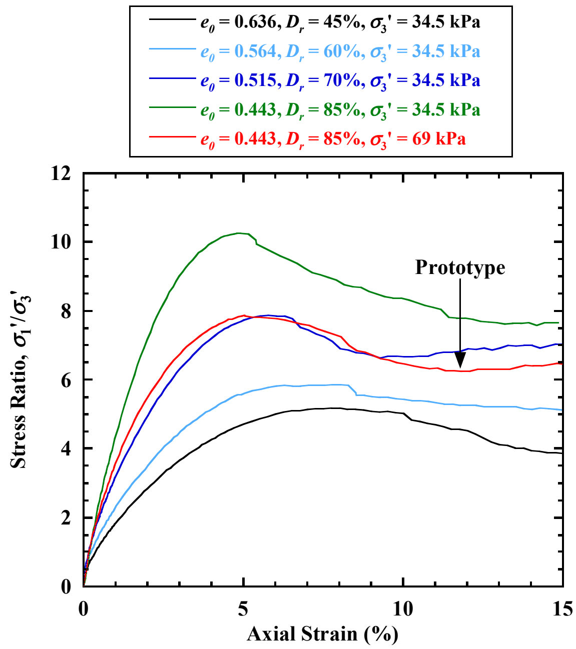

Figure 1. Five consolidated-drained triaxial compression tests on well-graded dry angular sand.

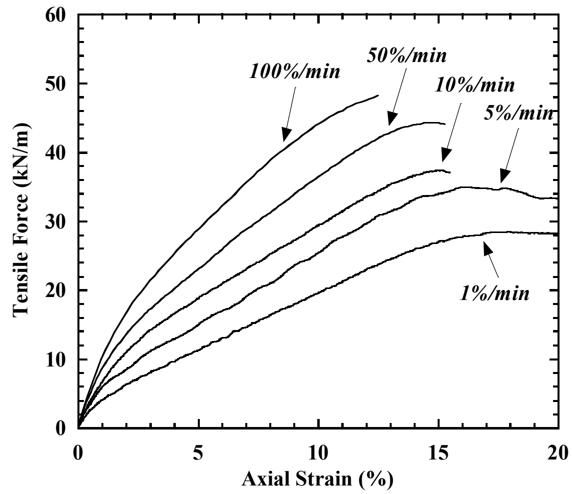

Figure 2. Tensile test results for HDPE geogrid (single rib specimens) at different strain rates.

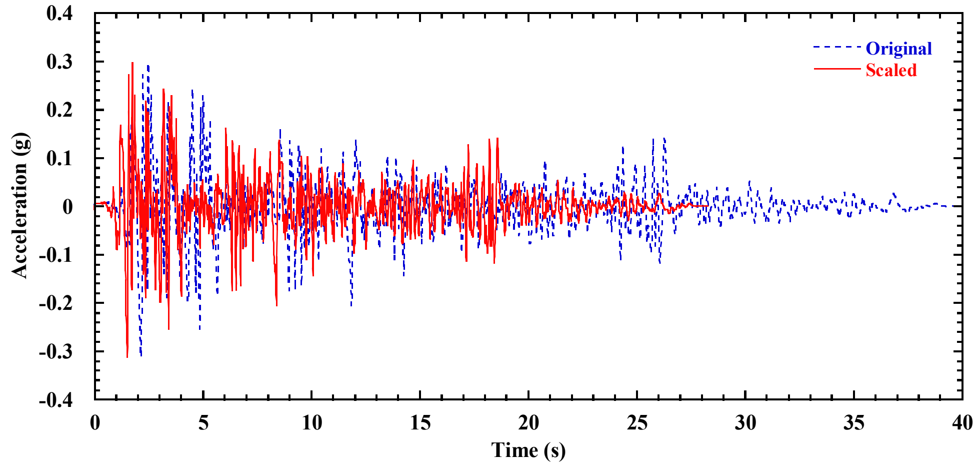

(a)

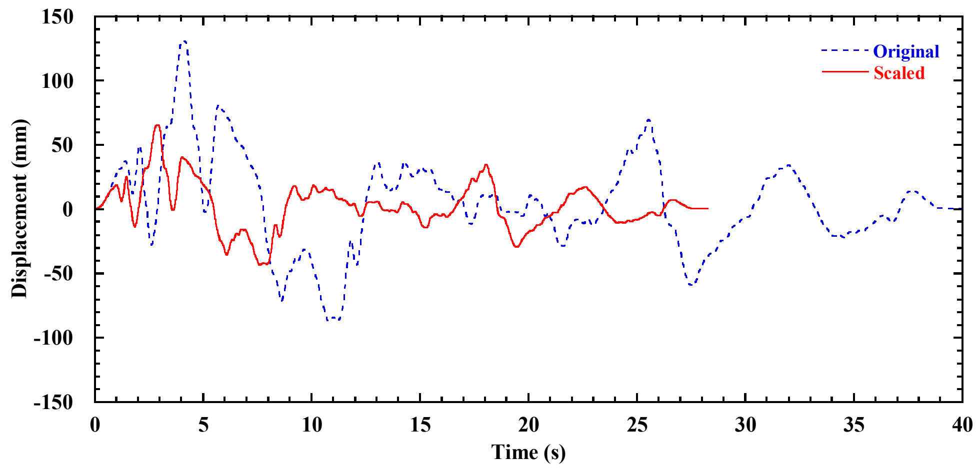

(b)

Figure 3. Original records and scaled motions for the 1940 Imperial Valley earthquake (El Centro station): (a) acceleration time history; (b) displacement time history.

Figure 4

Click here to access/download;Figure;Figure_4.pdf

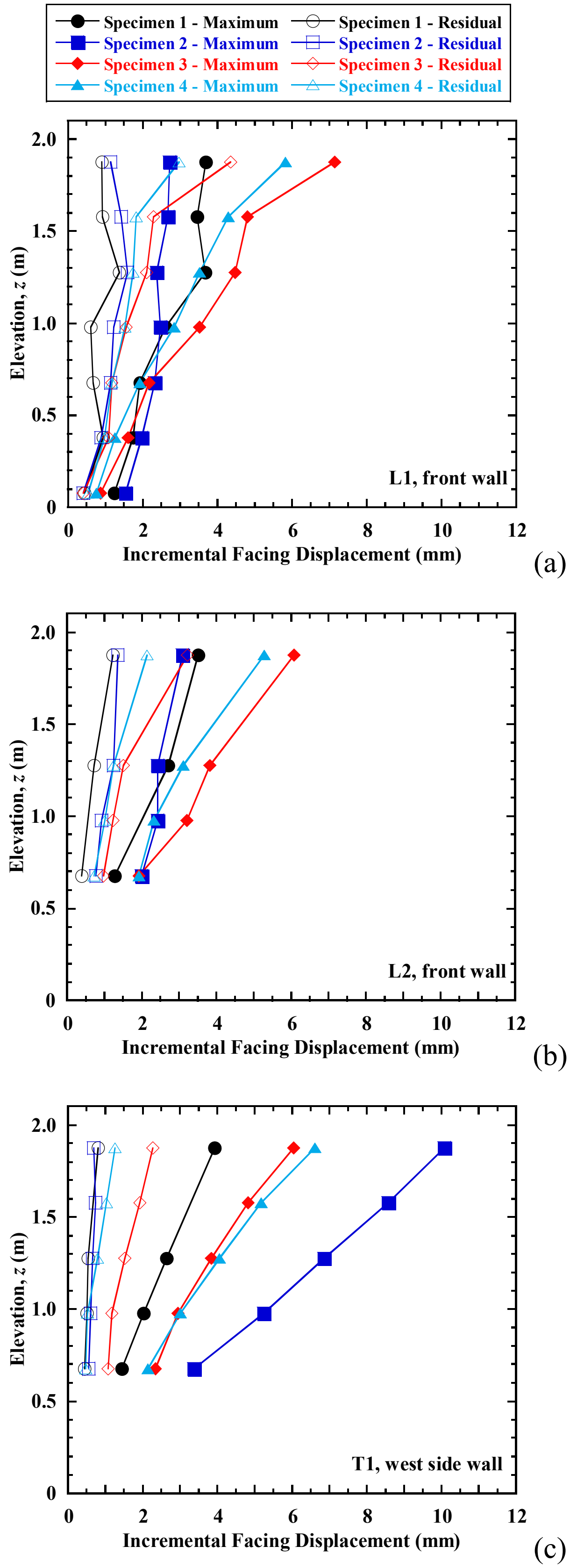

Figure 4. Profiles of incremental maximum and incremental residual facing displacement for the Imperial Valley motion: (a) L1, front wall; (b) L2, front wall; (c) T1, west side wall.

Figure 5 Click here to access/download;Figure;Figure_5.pdf

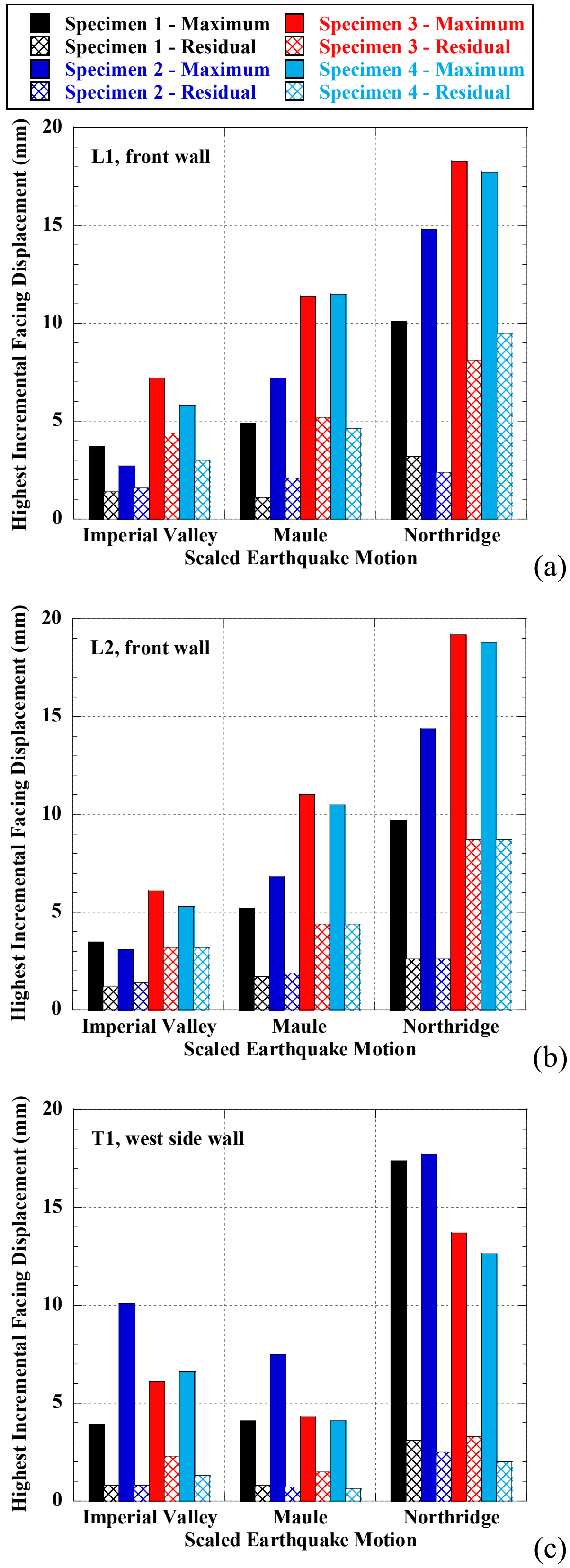

Figure 5. Highest values of incremental maximum and incremental residual facing displacement: (a) L1, front wall; (b) L2, front wall; (c) T1, west side wall.

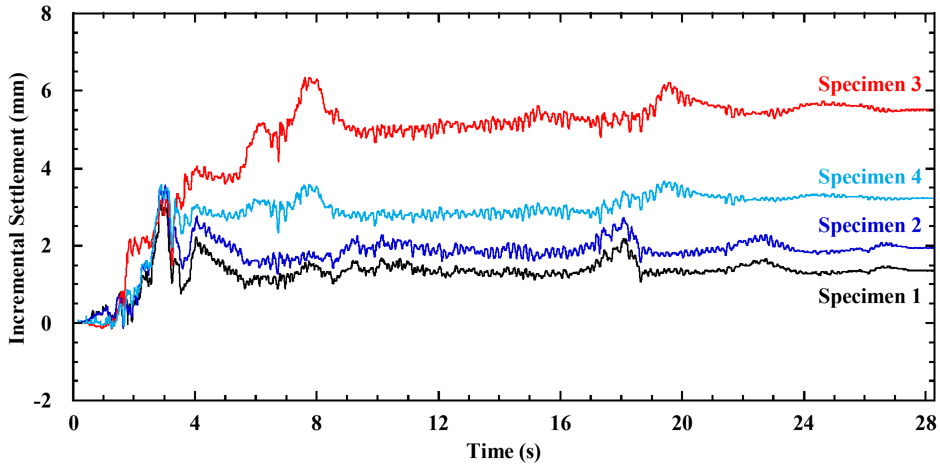

Figure 6. Time histories of average incremental bridge seat settlement during the Imperial Valley motion.

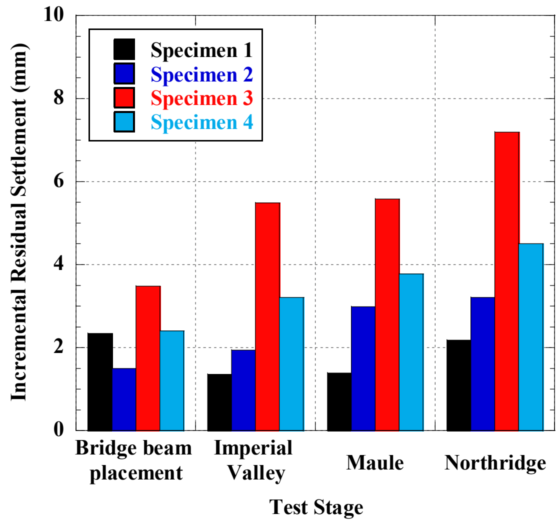

Figure 7. Average values of incremental residual bridge seat settlement.

Figure 8 Click here to access/download;Figure;Figure_8.pdf

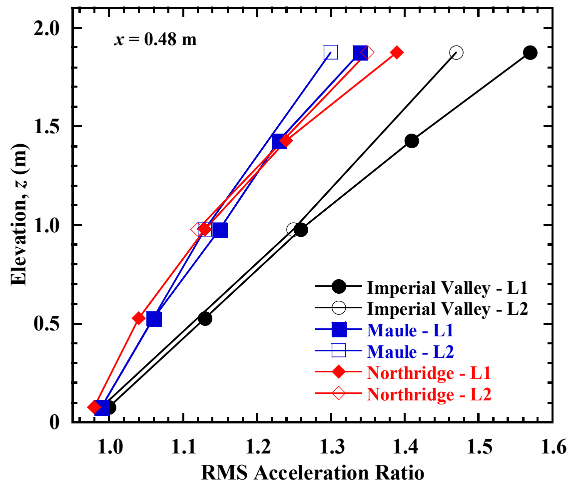

(a)

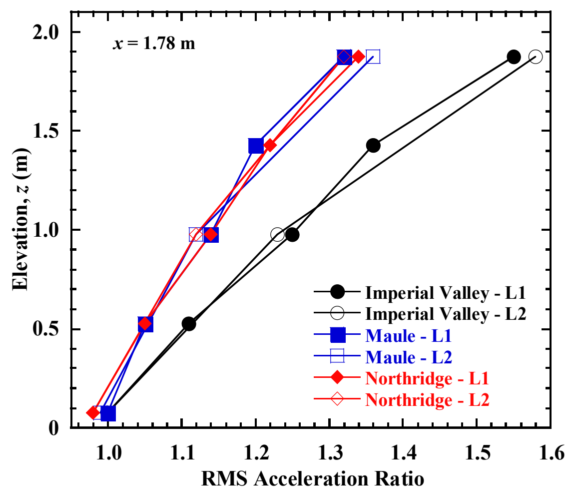

(b)

Figure 8. Profiles of RMS acceleration ratio for Specimen 1: (a) reinforced soil zone; (b) retained soil zone.

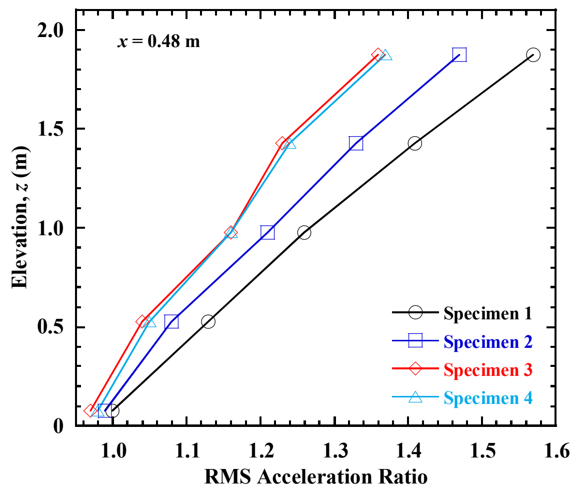

(a)

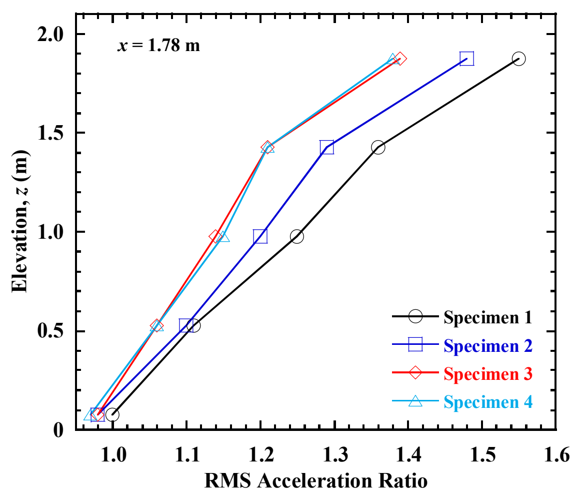

(b)

Figure 9. Profiles of RMS acceleration ratio for longitudinal section L1 during the Imperial Valley motion: (a) reinforced soil zone; (b) retained soil zone.

Figure 10 Click here to access/download;Figure;Figure_10.pdf

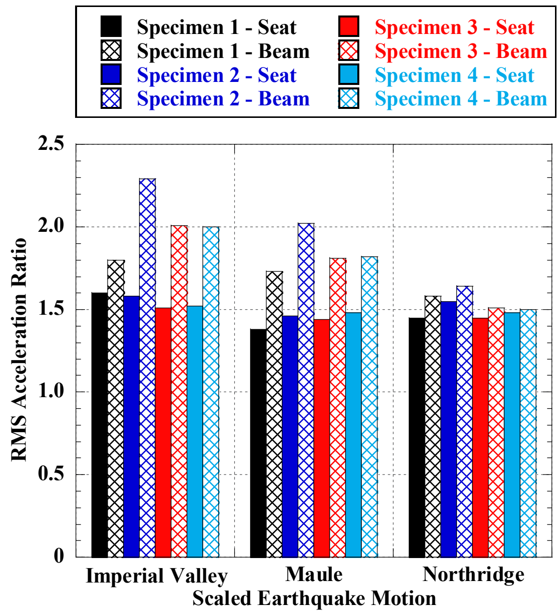

Figure 10. RMS acceleration ratios for specimen bridge seats and bridge beams during three scaled earthquake motions.

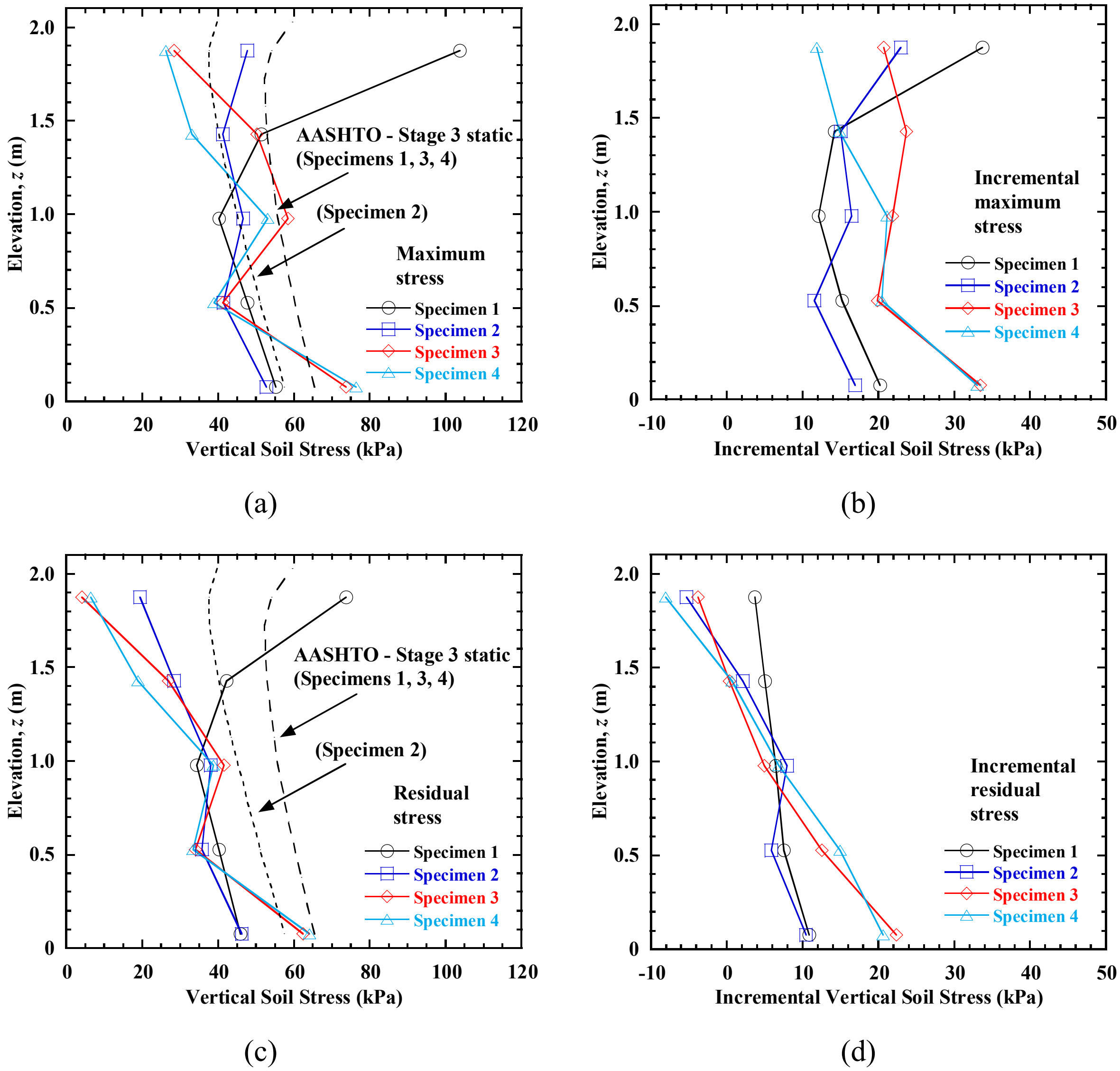

Figure 11. Profiles of vertical soil stress behind front wall facing for longitudinal section L1 and the Imperial Valley motion: (a) maximum; (b) incremental maximum; (c) residual; (d) incremental residual.

Figure 12 Click here to access/download;Figure;Figure_12.pdf

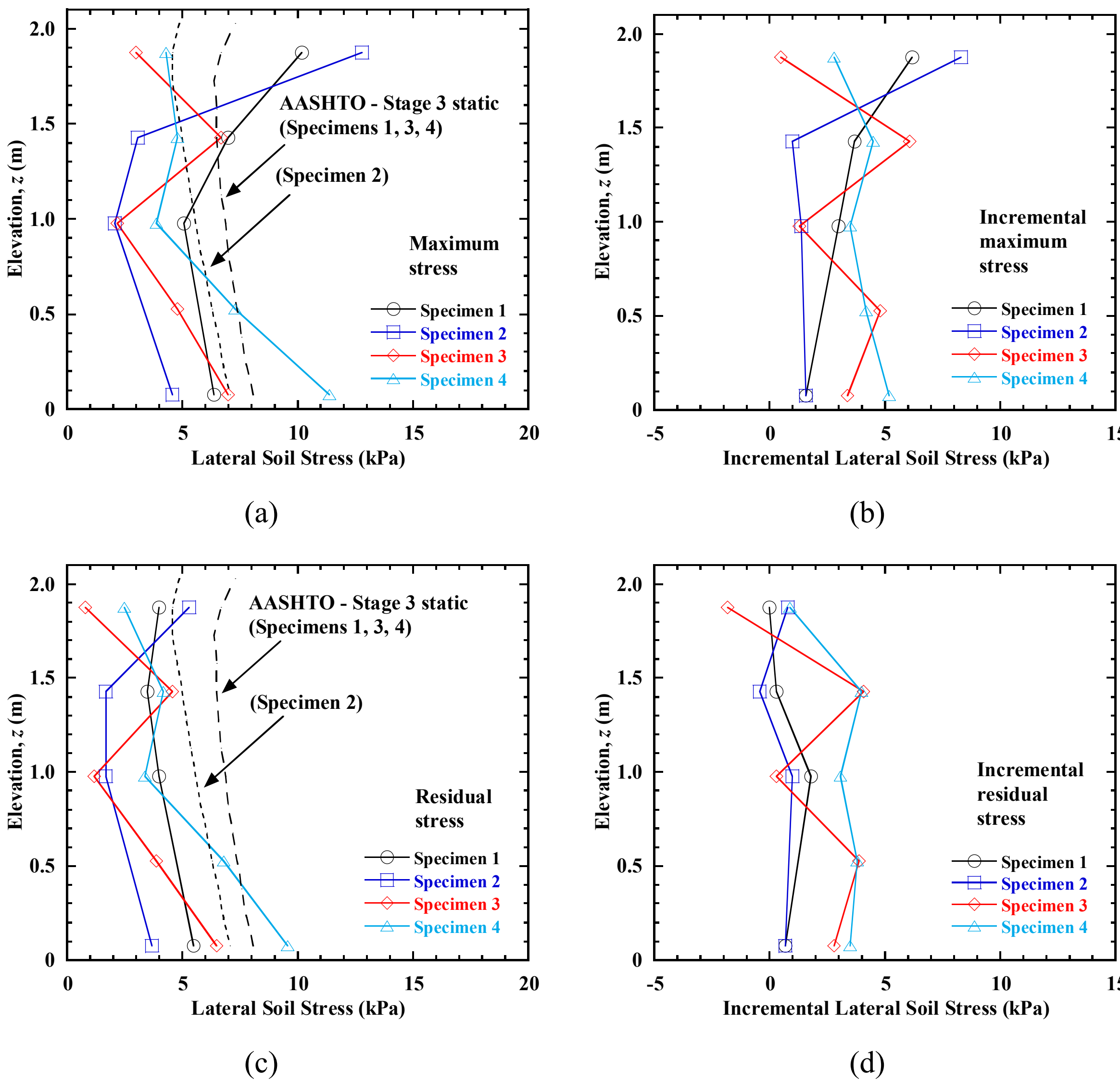

Figure 12. Profiles of lateral soil stress behind front wall facing for longitudinal section L1 and the Imperial Valley motion: (a) maximum; (b) incremental maximum; (c) residual; (d) incremental residual.

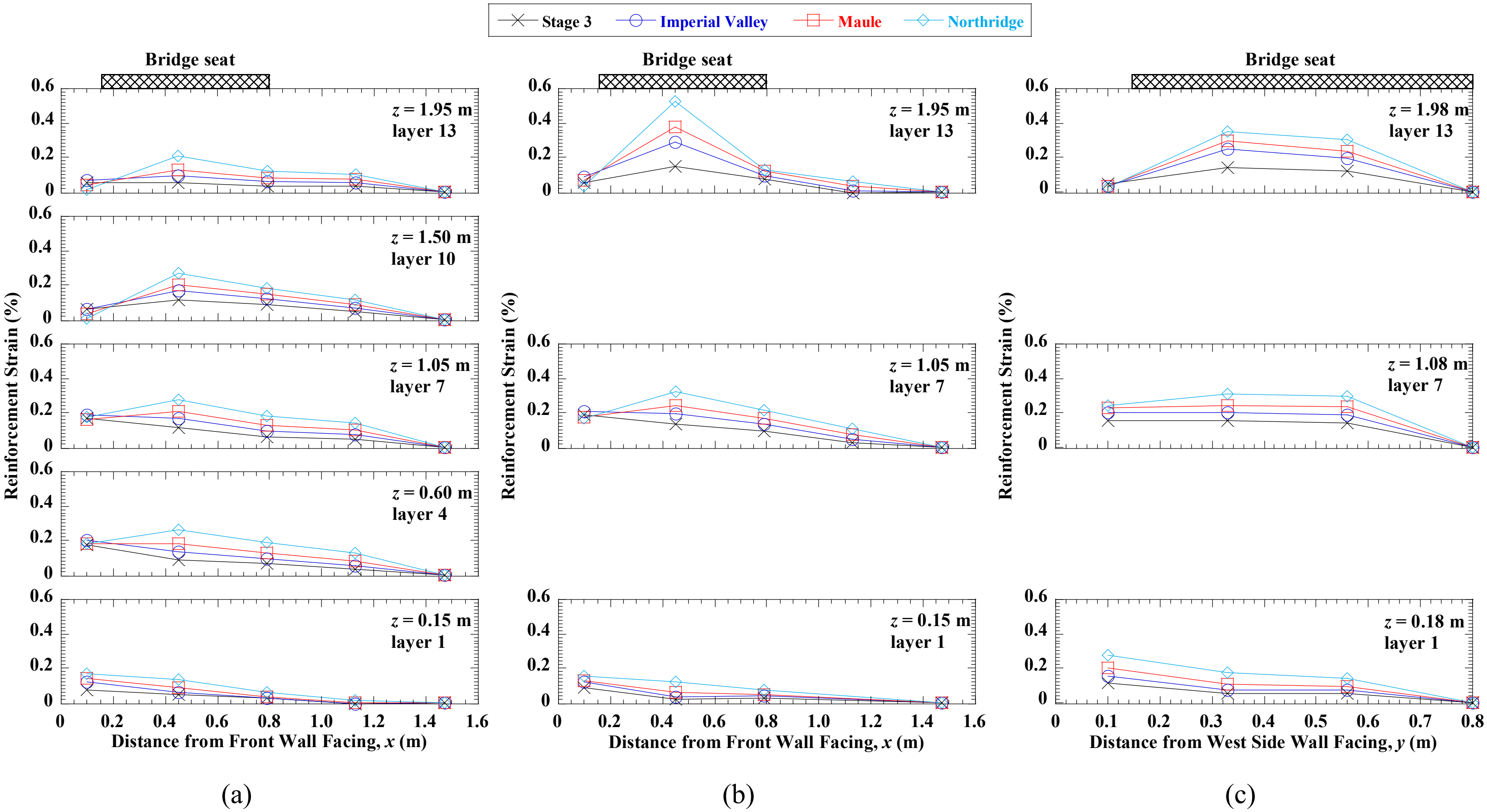

Figure 13. Distributions of residual tensile strain in reinforcement layers for Specimen 1: (a) L1; (b) L2; (c) T1.

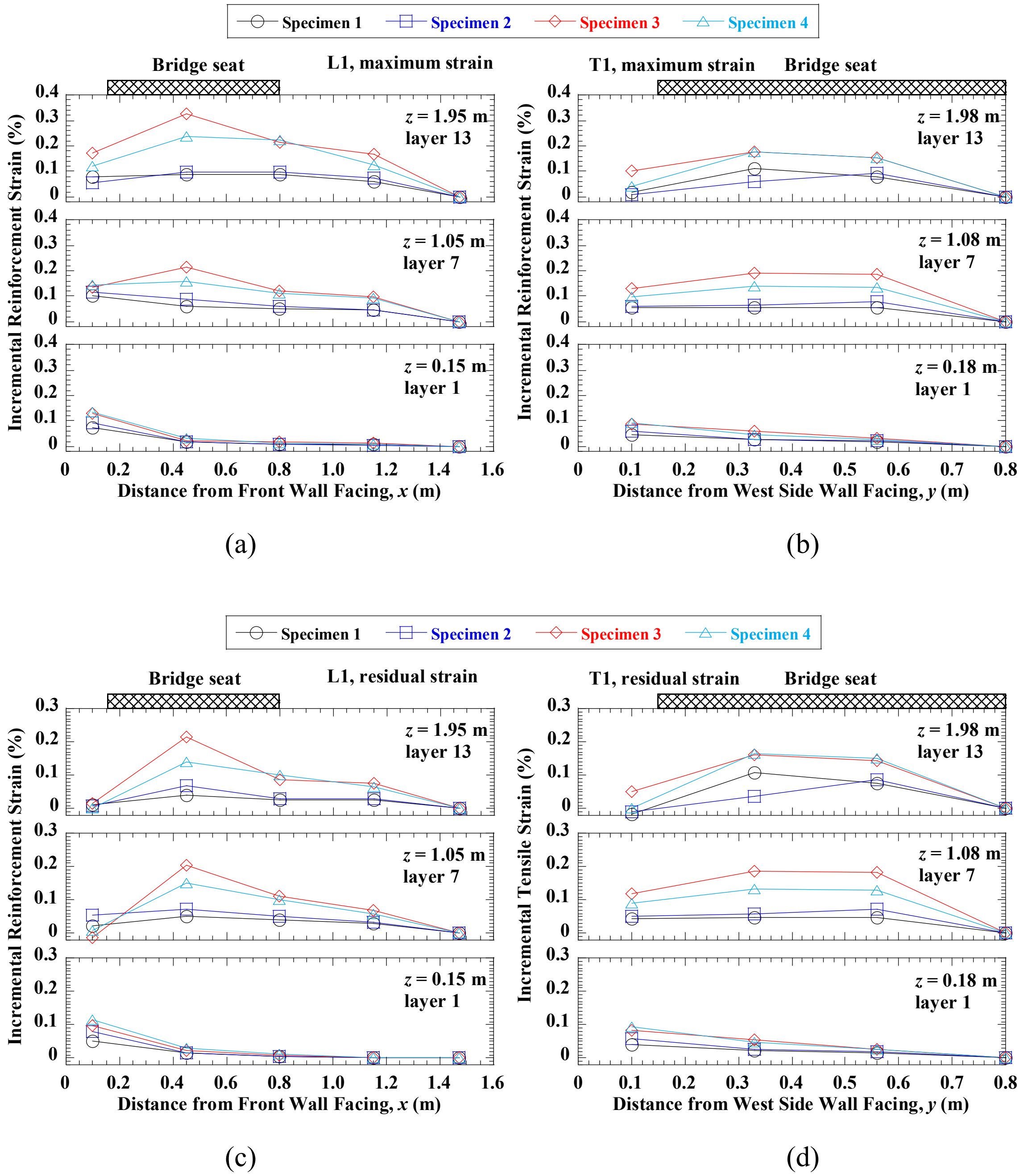

Figure 14. Distributions of incremental tensile strain in reinforcement layers for the Imperial Valley motion: (a) maximum for L1; (b) maximum for T1; (c) residual for L1; (d) residual for T1.

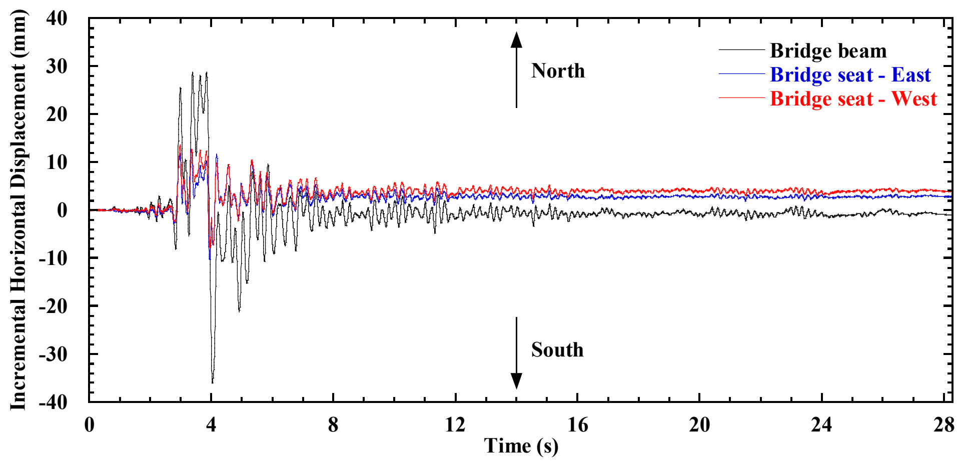

(a)

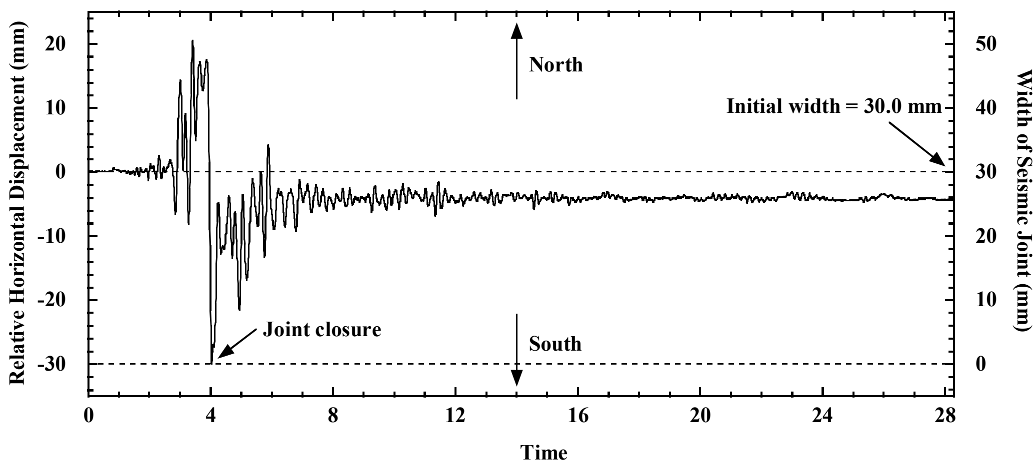

(b)

Figure 15. Time histories of bridge seat and bridge beam displacement for Specimen 1 during the Northridge motion: (a) incremental horizontal displacement; (b) relative horizontal displacement of bridge beam relative to the bridge seat.

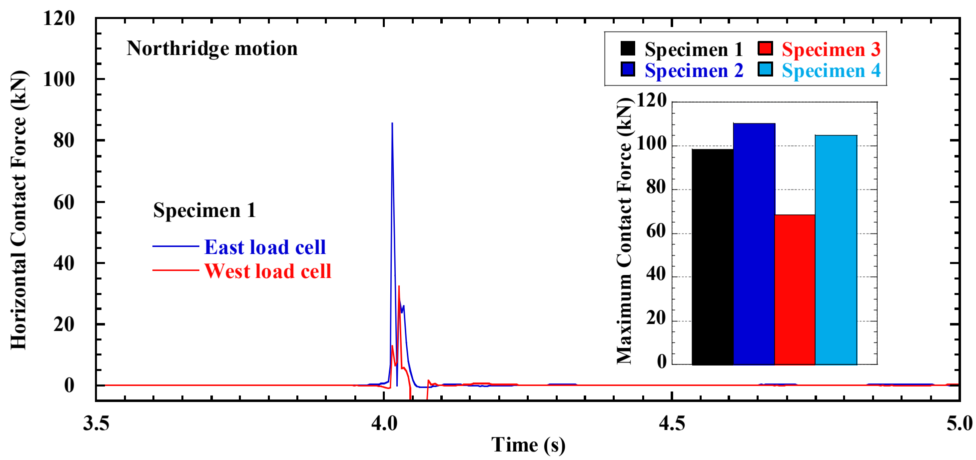

Figure 16. Time history of horizontal contact force between the bridge beam and bridge seat for Specimen 1 and maximum total contact forces during Northridge motion.

List of Figure Captions

Fig. 1. Five consolidated-drained triaxial compression tests on well-graded dry angular sand.

Fig. 2. Tensile test results for HDPE geogrid (single rib specimens) at different strain rates.

Fig. 3. Original records and scaled motions for the 1940 Imperial Valley earthquake (El Centro station): (a) acceleration time history; (b) displacement time history.

Fig. 4. Profiles of incremental maximum and incremental residual facing displacement for the Imperial Valley motion: (a) L1, front wall; (b) L2, front wall; (c) T1, west side wall.

Fig. 5. Highest values of incremental maximum and incremental residual facing displacement: (a) L1, front wall; (b) L2, front wall; (c) T1, west side wall.

Fig. 6. Time histories of average incremental bridge seat settlement during the Imperial Valley motion.

Fig. 7. Average values of incremental residual bridge seat settlement.

Fig. 8. Profiles of RMS acceleration ratio for Specimen 1: (a) reinforced soil zone; (b) retained soil zone.

Fig. 9. Profiles of RMS acceleration ratio for longitudinal section L1 during the Imperial Valley motion: (a) reinforced soil zone; (b) retained soil zone.

Fig. 10. RMS acceleration ratios for specimen bridge seats and bridge beams during three scaled earthquake motions.

Fig. 11. Profiles of vertical soil stress behind front wall facing for longitudinal section L1 and the Imperial Valley motion: (a) maximum; (b) incremental maximum; (c) residual; (d) incremental residual.

Fig. 12. Profiles of lateral soil stress behind front wall facing for longitudinal section L1 and the Imperial Valley motion: (a) maximum; (b) incremental maximum; (c) residual; (d) incremental residual.

Fig. 13. Distributions of residual tensile strain in reinforcement layers for Specimen 1: (a) L1; (b) L2; (c) T1.

Fig. 14. Distributions of incremental tensile strain in reinforcement layers for the Imperial Valley motion: (a) maximum for L1; (b) maximum for T1; (c) residual for L1; (d) residual for T1.

Fig. 15. Time histories of bridge seat and bridge beam displacement for Specimen 1 during the Northridge motion: (a) incremental horizontal displacement; (b) relative horizontal displacement of bridge beam relative to the bridge seat.

Fig. 16. Time history of horizontal contact force between the bridge beam and bridge seat for Specimen 1 and maximum total contact forces during Northridge motion.

ASCE Authorship, Originality, and Copyright Transfer Agreement

Publication Title: Journal of Geotechnical and Geoenvironmental Engineering

Manuscript Title: Physical Model Tests on Half-Scale Geosynthetic Reinforced Soil Bridge Abutments. II: Dynamic Loading

Author(s) – **Names, postal addresses, and e-mail addresses of all authors**

Yewei Zheng, Department of Structural Engineering, University of California, San Diego, La Jolla, CA, 92093-0085 USA. Email: y7zheng@ucsd.edu

Patrick J. Fox, Department of Civil and Environmental Engineering, Pennsylvania State University, University Park, PA, 16802 USA. Email: pjfox@engr.psu.edu

P. Benson Shing, Department of Structural Engineering, University of California, San Diego, La Jolla, CA, 92093-0085 USA. Email: pshing@ucsd.edu

John S. McCartney, Department of Structural Engineering, University of California, San Diego, La Jolla, CA, 92093-0085 USA. Email: mccartney@ucsd.edu

I. Authorship Responsibility

To protect the integrity of authorship, only people who have significantly contributed to the research or project and manuscript preparation shall be listed as coauthors. The corresponding author attests to the fact that anyone named as a coauthor has seen the final version of the manuscript and has agreed to its submission for publication. Deceased persons who meet the criteria for coauthorship shall be included, with a footnote reporting date of death. No fictitious name shall be given as an author or coauthor. An author who submits a manuscript for publication accepts responsibility for having properly included all, and only, qualified coauthors.

I, the corresponding author, confirm that the authors listed on the manuscript are aware of their authorship status and qualify to be authors on the manuscript according to the guidelines above.

Yewei Zheng	Yewei Zheng	06/04/18
Print Name	Signature	Date

II. Originality of Content

ASCE respects the copyright ownership of other publishers. ASCE requires authors to obtain permission from the copyright holder to reproduce any material that (1) they did not create themselves and/or (2) has been previously published, to include the authors' own work for which copyright was transferred to an entity other than ASCE. Each author has a responsibility to identify materials that require permission by including a citation in the figure or table caption or in extracted text. Materials re-used from an open access repository or in the public domain must still include a citation and URL, if applicable. At the time of submission, authors must provide verification that the copyright owner will permit re-use by a commercial publisher in print and electronic forms with worldwide distribution. For Conference Proceeding manuscripts submitted through the ASCE online submission system, authors are asked to verify that they have permission to re-use content where applicable. Written permissions are not required at submission but must be provided to ASCE if requested. Regardless of acceptance, no manuscript or part of a manuscript will be published by ASCE without proper verification of all necessary permissions to re-use. ASCE accepts no responsibility for verifying permissions provided by the author. Any breach of copyright will result in retraction of the published manuscript.

I, the corresponding author, confirm that all of the content, figures (drawings, charts, photographs, etc.), and tables in the submitted work are either original work created by the authors listed on the manuscript or work for which permission to re-use has been obtained from the creator. For any figures, tables, or text blocks exceeding 100 words from a journal article or 500 words from a book, written permission from the copyright holder has been obtained and supplied with the submission.

Yewei Zheng	Yewei Zheng	06/04/18
Print name	Signature	Date

III. Copyright Transfer

ASCE requires that authors or their agents assign copyright to ASCE for all original content published by ASCE. The author(s) warrant(s) that the above-cited manuscript is the original work of the author(s) and has never been published in its present form.

The undersigned, with the consent of all authors, hereby transfers, to the extent that there is copyright to be transferred, the exclusive copyright interest in the above-cited manuscript (subsequently called the "work") in this and all subsequent editions of the work (to include closures and errata), and in derivatives, translations, or ancillaries, in English and in foreign translations, in all formats and media of expression now known or later developed, including electronic, to the American Society of Civil Engineers subject to the following:

- The undersigned author and all coauthors retain the right to revise, adapt, prepare derivative works, present orally, or distribute the work, provided that all such use is for the personal noncommercial benefit of the author(s) and is consistent with any prior contractual agreement between the undersigned and/or coauthors and their employer(s).
- No proprietary right other than copyright is claimed by ASCE.
- If the manuscript is not accepted for publication by ASCE or is withdrawn by the author prior to publication (online or in print), or if the author opts for open-access publishing during production (journals only), this transfer will be null and void.
- Authors may post a PDF of the ASCE-published version of their work on their employers' ***Intranet*** with password protection. The following statement must appear with the work: "This material may be downloaded for personal use only. Any other use requires prior permission of the American Society of Civil Engineers."
- Authors may post the ***final draft*** of their work on open, unrestricted Internet sites or deposit it in an institutional repository when the draft contains a link to the published version at www.ascelibrary.org. "Final draft" means the version submitted to ASCE after peer review and prior to copyediting or other ASCE production activities; it does not include the copyedited version, the page proof, a PDF, or full-text HTML of the published version.

Exceptions to the Copyright Transfer policy exist in the following circumstances. Check the appropriate box below to indicate whether you are claiming an exception:

☐ **U.S. GOVERNMENT EMPLOYEES:** Work prepared by U.S. Government employees in their official capacities is not subject to copyright in the United States. Such authors must place their work in the public domain, meaning that it can be freely copied, republished, or redistributed. In order for the work to be placed in the public domain, ALL AUTHORS must be official U.S. Government employees. If at least one author is not a U.S. Government employee, copyright must be transferred to ASCE by that author.

☐ **CROWN GOVERNMENT COPYRIGHT:** Whereby a work is prepared by officers of the Crown Government in their official capacities, the Crown Government reserves its own copyright under national law. If ALL AUTHORS on the manuscript are Crown Government employees, copyright cannot be transferred to ASCE; however, ASCE is given the following nonexclusive rights: (1) to use, print, and/or publish in any language and any format, print and electronic, the above-mentioned work or any part thereof, provided that the name of the author and the Crown Government affiliation is clearly indicated; (2) to grant the same rights to others to print or publish the work; and (3) to collect royalty fees. ALL AUTHORS must be official Crown Government employees in order to claim this exemption in its entirety. If at least one author is not a Crown Government employee, copyright must be transferred to ASCE by that author.

☐ **WORK-FOR-HIRE:** Privately employed authors who have prepared works in their official capacity as employees must also transfer copyright to ASCE; however, their employer retains the rights to revise, adapt, prepare derivative works, publish, reprint, reproduce, and distribute the work provided that such use is for the promotion of its business enterprise and does not imply the endorsement of ASCE. In this instance, an authorized agent from the authors' employer must sign the form below.

☐ **U.S. GOVERNMENT CONTRACTORS:** Work prepared by authors under a contract for the U.S. Government (e.g., U.S. Government labs) may or may not be subject to copyright transfer. Authors must refer to their contractor agreement. For works that qualify as U.S. Government works by a contractor, ASCE acknowledges that the U.S. Government retains a nonexclusive, paid-up, irrevocable, worldwide license to publish or reproduce this work for U.S. Government purposes only. This policy DOES NOT apply to work created with U.S. Government grants.

I, the corresponding author, acting with consent of all authors listed on the manuscript, hereby transfer copyright or claim exemption to transfer copyright of the work as indicated above to the American Society of Civil Engineers.

Yewei Zheng

Print Name of Author or Agent

Yewei Zheng 06/04/18

Signature of Author of Agent Date

More information regarding the policies of ASCE can be found at http://www.asce.org/authorsandeditors

Authors: Zheng, McCartney, Shing, and Fox
Technical Paper: JGGE GTENG 7259
Title: Physical Model Tests of Half-Scale Geosynthetic Reinforced Soil Bridge Abutments. II: Dynamic Loading
Date: April 2019

Response to Review Comments

Editor:

I received your first revised manuscript titled: "Physical Model Tests on Half-Scale Geosynthetic Reinforced Soil Bridge Abutments. II: Dynamic Loading" (GTENG-7259-R1) for possible publication in the ASCE Journal of Geotechnical and Geoenvironmental Engineering (JGGE). Your Technical Paper (TP) presents the results of shake table tests on four half-scale geosynthetic reinforced soil (GRS) bridge abutments to investigate the effects of seismic surcharge, reinforcement spacing, and reinforcement stiffness on the seismic behavior of GRS bridge abutments. The results produced some new data on wall lateral displacement, bridge settlement, and increases in vertical and lateral stresses due to shaking, which should be of interest to practitioners.

Three (3) highly active reviewers in this field have reviewed your manuscript and their extensive review comments are provided below. Based on the review comments, the Associate Editor (AE) recommended that your revised manuscript be "Revise for Re-Review by Editor Only".

As an Editor of the JGGE, I also have reviewed your TP great interest in the subject matter and concur with the AE's recommendation because Reviewers #1 and #3 have requested some additional changes and clarifications to your TP.

As a result, I recommend that your paper be "Revised for Editor Only" and the AE and I will review the revised manuscript to ensure that my comments and the comments of Reviewer #1 and #3 have been adequately addressed. Please carefully address all of the review comments, especially Reviewer #3, and provide a TABULATED point-by-point response along with your revised manuscript.

> *Response: We value these comments and have improve the manuscript. Please see our response to comments below.*

Associate Editor:

Two of the three reviewers still have some comments on this manuscript. The comments are mostly related to the clarifications of some details. The authors are encouraged to address these comments by providing more details. Since these two companion papers will be published together if both are accepted, there is no need to repeat figures and tables as suggested by Reviewer #1.

> *Response: We have addressed the additional comments from the two reviewers. As part of our revision, we have minimized any redundancy between the two companion papers. There are no repeated figures or tables in the two papers.*

Reviewer #1:

As there are only limited studies carried out on the seismic response of GRS-IBS, I believe this article will give meaningful insights on the behavior of GRS abutments under dynamic loads.
There are too many cross references between two companion papers. In the sections of "specimen configuration" and "soil and reinforcement", if the authors gave the figures, tables and material properties, that's enough so that it is not necessary to refer the companion paper. In the configuration of specimens, the retained soil was reinforced by transverse uniaxial geogrid. Could the authors explain any effects on the measured acceleration in retained soils by this arrangement?

> *Response: Thank you for your review. As noted in the response above, we have minimized any cross references between the companion papers. In general, the measured acceleration amplification ratios in the direction of shaking for the reinforced soil zone and retained soil zone are nearly the same at different elevations. Since earthquake motions were applied in the longitudinal direction, the transverse reinforcement layers would not be expected to significantly affect the dynamic behavior for shaking in the longitudinal direction, as the tensile stiffness in the cross-machine direction is much lower than that in the machine-direction.*

Reviewer #3:

The authors did an outstanding job in addressing the majority of the reviewer's comments and in improving their manuscript. The reviewer hopes that the provided comments were found useful by the authors in improving the technical content of their manuscript. The reviewer, however, is afraid some important comments may still have not been addressed in full or in part. Following is the reviewer's reinstated comments (comment numbers are the same as those used by the authors in their responses):

Response: Thank you. We have addressed the following additional comments and improved the manuscript.

11. The authors explained how the applied the scaling factors presented in Table 1 on their identification of the material properties (fill and reinforcement). The explanation, however, still lacks the explanation of how changing the material density (scaling factor = 1) renders the same soil stiffness and strength (scaling factor = 2) considering the scaling factors reported in Table 1. Additional clarification from the authors will be much appreciated and would reduce the ambiguity.

Response: The Iai (1989) similitude relationships define three independent scaling factors for length, density, and strain to ensure a similar stress-strain response between model and prototype. The scaling factors for density and strain typically are assumed as unity for a given soil, leaving the length scaling factor as the main consideration. In our study, a length scaling factor of λ *= 2 was used to design the half-scale GRS bridge abutment specimens. A relative density* D_r *= 85% was chosen for the prototype abutment structure, which corresponds to a relative compaction of 96% and meets field compaction requirements for GRS bridge abutments (Berg et al. 2009; Adams et al. 2011). Once the prototype relative density was established, consolidated-drained (CD) triaxial compression tests were conducted to determine the target relative density for construction of the half-scale GRS abutment specimens. Measured relationships for stress ratio* σ_1'/σ_3' *versus axial strain from five CD triaxial tests on dry sand specimens are shown in the figure below. An initial test was conducted for* D_r *= 85% (initial void ratio* e_o *= 0.443) and effective confining stress* σ_3' *= 69.0 kPa to provide the average stress-strain response of the backfill soil at the mid-height of a prototype structure. Using the stress scaling factor (2) in Table 1 of the manuscript, four additional CD triaxial tests were conducted for* σ_3' *= 34.5 kPa and* D_r *= 45%, 60%, 70%, and 85%. The relationship for* D_r *= 70% and* σ_3' *= 34.5 kPa yielded similar stiffness and strength to that for the prototype and, as such, a value of* D_r *= 70% was chosen for construction the half-scale abutment specimens. The corresponding density ratio for the 85%/69.0 kPa and 70%/34.5 kPa specimens is 1.05 (= 1808 kg/m*^{3}*/1722 kg/m*^{3}*) and the strain ratio at peak is 0.87 (= 5.05%/5.79%), which are small deviations from the theoretical values of unity in Table 1 of the manuscript. Explanation was added to the revised manuscript.*

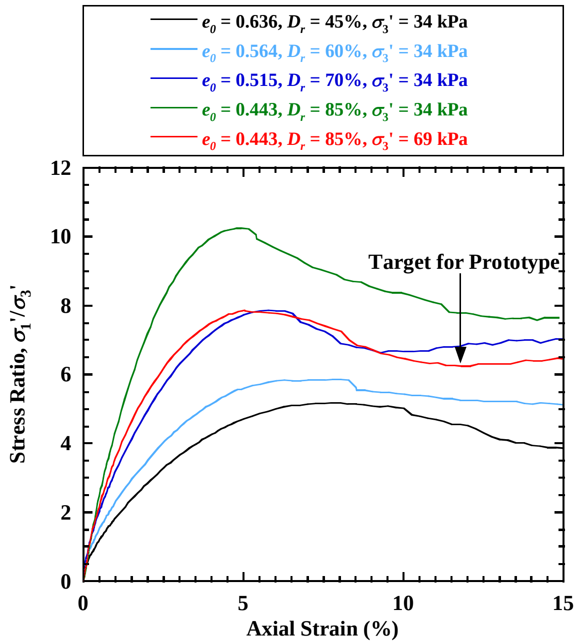

20. The authors in their response referred to the brand name of the pressure cells used but not the type. The reviewer still thinks that it is important to know and report the type of pressure cell in the manuscript. Pressure cells are challenging to rely on in geotechnical engineering. For instance, if the authors used vibrating wire pressure cells, corrections may be needed to account for the interference with the imposed vibrations from the test input motions. A disclaimer statement is needed in the manuscript to inform the readers with the simplifications that may have been made by the authors in treating the output readings of the pressure cells.

> *Response: According to the information from the manufacturer, it is a load cell-based contact earth pressure cells, with capacities of 160 kPa and 320 kPa. The pressure cells were used successfully for investigation of static and dynamic soil-structure interaction in previous studies and do not require special correction for dynamic testing (e.g., Fox et al. 2015; Keykhosropour et al. 2018). This information was added to the revised manuscript.*

49. The authors explained that the large difference between the load cells readings shown in Figure 16 is because the tips of the load cells were not perfectly parallel with respect to the bridge seat. It would be clearer to the readers if the authors state this justification in the manuscript, so the readers can understand the difference observed in the figure.

> *Response: Clarification added to the revised manuscript.*

96. Add reference/source to Table 2 caption (PEER Ground Motion Database …?).

Response: The earthquake motions in this study are scaled, not the original data from PEER Ground Motion Database. We believe that it is sufficient to cite the motion database only when mentioning the source of the unscaled motions.

References

Adams, M., Nicks, J., Stabile, T., Wu, J., Schlatter, W., and Hartmann, J. (2011). "Geosynthetic reinforced soil integrated bridge system interim implementation guide." *FHWA-HRT-11-026*, U.S. DOT, Washington, D.C.

Berg, R.R., Christopher, B.R., and Samtani, N. (2009). "Design and construction of mechanically stabilized earth walls and reinforced soil slopes – Volume I." *FHWA-NHI-10-024*, U.S. DOT, Washington, D.C.

Fox, P.J., Andrew, A.C., Elgamal, A., Greco, P., Isaacs, D., Stone, M., and Wong, S. (2015). "Large soil confinement box for seismic performance testing of geo-structures." *Geotechnical Testing Journal*, 38(1), 72-84.

Iai, S. (1989). "Similitude for shaking table tests on soil-structure-fluid models in 1 g gravitational fields." *Soils and Foundations*, 29(1), 105-118.

Keykhosropour, L., Lemnitzer, A., Star, L., Marinucci, A., and Keowen, S. (2018). "Implementation of soil pressure sensors in large-scale soil-structure interaction studies," *Geotechnical Testing Journal*, 41(4), 730–746.